

# Integration of single-nuclei transcriptome and bulk RNA-seq to unravel the role of *AhWRKY70* in regulating stem cell development in *Arachis hypogaea* L.

Xinyang Wang<sup>1,2,†</sup>, Runfeng Wang<sup>1,†</sup>, Xing Huo<sup>3,†</sup>, Yueni Zhou<sup>1,†</sup>, Muhammad J. Umer<sup>1</sup>, Zihao Zheng<sup>4</sup>, Weicai Jin<sup>1</sup>, Lu Huang<sup>1</sup>, Haifen Li<sup>1</sup>, Qianxia Yu<sup>1</sup>, Shaoxiong Li<sup>1</sup>, Rajeev K Varshney<sup>5</sup> , Wenyi Wang<sup>6</sup> , Yuan Xiao<sup>7</sup>, Yanbin Hong<sup>1,\*</sup>, Xiaoping Chen<sup>1,\*</sup>, Qing Lu<sup>1,\*</sup> and Hao Liu<sup>1,\*</sup> 

<sup>1</sup>Crops Research Institute, Guangdong Academy of Agricultural Sciences, Guangdong Provincial Key Laboratory of Crop Genetic Improvement, South China Peanut Sub-Center of National Center of Oilseed Crops Improvement, Guangzhou, Guangdong, China

<sup>2</sup>College of Traditional Chinese Medicine, Bozhou University, Bozhou, Anhui, China

<sup>3</sup>Rice Research Institute Guangdong Academy of Agricultural Sciences, Guangdong Academy of Agricultural Sciences, Guangzhou, Guangdong, China

<sup>4</sup>Department of Agronomy, Iowa State University, Ames, IA, USA

<sup>5</sup>State Agricultural Biotechnology Centre, Centre for Crop and Food Innovation, Food Futures Institute, Murdoch University (MU), Murdoch, WA, Australia

<sup>6</sup>College of Agriculture, South China Agriculture University, Guangzhou, Guangdong, China

<sup>7</sup>School of Public Health, Wannan Medical College, Wuhu, Anhui, China

Received 13 July 2024;  
revised 15 November 2024;  
accepted 2 February 2025.

\*Correspondence (Tel +86 020 87511794; fax +86 020 85514269; email liuhao@gdaas.cn (H.L.), Tel +86 020 38289853; fax +86 020 85514269; email hongyanbin@gdaas.cn (Y.H.), Tel +86 020 38085534; fax +86 020 85514269; email chenxiaoping@gdaas.cn (X.C.), Tel +86 020 87511794; fax +86 020 85514243; email luqing@gdaas.cn (Q.L.))

†These authors contributed equally to this work.

## Summary

Peanut stem is a vital organ to provide mechanical support and energy for aerial tissue development. However, the transcriptional regulatory mechanisms underlying stem development at a single-cell resolution remain unclear. Herein, single-nuclei isolation coupled with fluorescent-activated cell sorting was employed to construct a cell atlas of peanut seedling stems using microdroplets-based single-nuclei RNA-sequencing. This approach yielded 29 308 cells with 53 349 expressed genes underlying the identification of five cell types characterized by known marker genes. Additionally, 2053 differentially expressed genes (DEGs) were identified across different cell types. Furthermore, 3306 core-DEGs involved in cell development trajectories were used to construct a transcription factor (TF) interaction network, providing insights into specific biological pathways and transcriptional regulation dynamics underlying cell-type differentiation. Additionally, 1446 DEGs associated with different cell-cycle profile were identified, revealing that peanut stem elongation and cell expansion are closely linked to auxin-responsive pathway. This was supported by the examination of endogenous phytohormones and the identification of 10 hormone-responsive DEGs. Moreover, *AhWRKY70* was localized in the nucleus and is highly enriched in stem cortex and xylem cells and exhibits a tissue-specific expression pattern that regulates stem growth. Overexpression of *AhWRKY70* in *Arabidopsis* led to accelerated stem growth by modulating the phytohormone signalling pathway, influencing the expression of sixteen auxin and ethylene-responsive genes as demonstrated by transcriptome sequencing. In conclusion, the single-cell atlas provides a foundational dataset for understanding gene expression heterogeneity in peanut seedling stems. The elucidation of *AhWRKY70* function expands our understanding of the roles of WRKY family members in peanut.

**Keywords:** peanut seedling, single-nuclei RNA-seq (snRNA-seq), stem growth, WRKY protein, phytohormone.

## Introduction

Peanut (*Arachis hypogaea* L.) is a pivotal multi-purpose oil-seed legume, whose seeds provide a resource for edible oil and nutritious protein. Peanut is likely originated from a hybridization event between its two progenitors, *Arachis duranensis* and *Arachis ipaensis* in South America. It was domesticated ~6000 years ago and has since been widely dispersed during post-Columbian times (Chen *et al.*, 2019) in breeding. To compare the peanut progenitors, cultivated varieties are divided into distinct market types based on their stem-determined plant architecture, such as the Spanish type (small pod, upright branches), Runner type (sarmentious branches) and Virginia type (large pod, erect or sarmentious

branches) ([www.peanutgr.fafu.edu.cn](http://www.peanutgr.fafu.edu.cn)). Therefore, the stem is an important organ that affects the peanut growth (Zang *et al.*, 2023). During the seedling stage, when the peanut plant breaks through the soil, the stem provides mechanism support for aerial tissues growth and is responsible for energy transport and nutrient exchange. Despite the establishment of transcriptomes for distinct peanuts organs at the tissue level to identify stem-specific gene expression profiles (Sinha *et al.*, 2020) the transcriptional regulatory mechanisms of stem cell development at a single-cell resolution remain unclear. An illustration of the stem cell atlas could enhance our understanding of peanut architecture and growth, thereby accelerating and promoting further functional genes validation in specific cell types of peanut stem.

The primary functions of the stem are to support the leaves, allowing them to obtain water and minerals for energy production via photosynthesis and to transport these products from the leaves to other parts of the plant, including the roots. The stem conducts water and nutrient minerals from their site of absorption in the roots to the leaves by means of certain vascular tissues in the xylem. The movement of synthesized nutrient substances from the leaves to other plant organs occurs chiefly through other vascular tissues in the phloem (Greb and Lohmann, 2016). Additionally, plant stem is one of nature's most impressive mechanical constructs. Their sophisticated hierarchical structure and multifunctionality allow plant from the integral level of stem structures develops down to the fibre-reinforced composite character of the cell walls (Hunziker and Greb, 2024). Stem height is a major factor in artificially regulating plant architecture, determining the spatial distribution of other organs by manipulating a series of dwarf genes that interact with various phytohormone pathways, such as gibberellin, brassinolide and cytokinin, especially the *SD1* gene (Kuroha et al., 2018) induced semi-dwarf stem trait with high yield triggered green revolution. Stem cells originate from the shoot apical meristem (SAM) until seed germination, involving typical homeodomain TFs like SHOOTMERISTEMLESS (STM) (Balkunde et al., 2017) and WUSCHEL (WUS) (Jha et al., 2020) which are located in the organizing centre (OC) to modulate differentiation procedures and maintain the proliferative capacity of meristematic cells, converting them into stem cells through the CLAVATA3 (CLV3) and CLV1/2-derived peptide cascade signal (Hirakawa, 2021). Meanwhile, stem produces an influence on multiple-tissue formation with molecular transcriptional regulation, including the branch growth angle, lateral bud inhibition and repression, and flower bud differentiation. However, above-mentioned molecular mechanism illustration-associated stem morphology observations are limited to tissue level. Further exploring the gene expression profile on single-cell level could provide novel biological insights into stem cell development.

Currently, single-cell RNA sequencing (scRNA-seq) technology provides unprecedented opportunities to decipher the spatio-temporal complexity of plant growth and development at the individual cell resolution. Plant single-cell transcriptomics relies on protoplast cell isolation and single-nucleus capture methods, both of which combine with microdroplet-based library construction to describe the gene expression profile in specific cell types. Previously, we utilized scRNA-seq based on protoplast cell to describe single-cell transcriptome in peanut seedling leave blade and established the TFs interaction network (Liu et al., 2021a). In another study, scRNA-seq (protoplast cell system) was used to reveal the cytokinin-repressed mechanism that slows leaf development in high-oleic acid peanut varieties (Du et al., 2023). Additionally, we provided different single-cell transcriptome atlases of peanut seedlings responding to distinct light conditions (Deng et al., 2024). Recently, due to the barriers of enzymolysis protoplast capture that exist in the tissue with higher lignification cell wall, we developed a single-nucleus atlas of transcriptome and chromatin accessibility in the same individual cell in the peanut leaves using fluorescence-activated and sorted single nuclei. Our previous studies have accelerated the progress of single-cell transcriptome development in peanuts and provided a technological foundation for conducting scRNA-seq in various peanut tissues (Liao and Wang, 2023;

Rodriguez-Villalon and Brady, 2019; Ryu et al., 2021; Shaw et al., 2021).

Peanut stem controls the several agronomic traits with distinct phenotypes, such as erect growth (V type), semi-sarmentous growth (U type) and horizontal creep growth (T type). In this study, to obtain the stem cell atlas on individual-cell level, we used fluorescence-activated nucleus sorting (FANS) and a micro-droplet platform to establish a stable single-nucleus isolation approach for peanut stem. Furthermore, high-throughput snRNA-seq was employed to characterize the transcriptome in stem cell. This transcriptome atlas, integrated with tissue bulk RNA-seq, helped identify the transcriptional molecular dynamics of gene expression from the tissue level to single-cell resolution. These multi-dimensions transcriptome data revealed critical single-cell differentiation trajectories and provided novel biological insights into leguminous stem development.

## Results

### snRNA-seq reveals cell clusters and transcriptome atlas in peanut stem cell

To obtain the single-cell transcriptome atlas in peanut stem, a robust tissue nuclei isolation method was developed to capture the single-cell nuclei with DAPI staining, and pure single-nuclei suspension was obtained after the process of FANS filtering then loaded into 10 $\times$  genomics microfluidic platform to generate the micro-droplets and sequencing library (Figure 1a; Table S1). Totally, the snRNA-seq identified 29 308 single-cells (Table S2) in peanut stem by reading the barcode and UMI sequence (Figure S1), further visualization of the cells distribution using Stochastic neighbour embedding (t-SNE) revealed all independent cells can be divided into 18 cell clusters (Figure 1b; Figure S2). scRNA-seq identified a total of 53 349 expressed genes (Table S3), of which 4097 differentially expressed genes (DEGs) exhibited significant expression level in different cell clusters (Table S4, Figure S3A), suggesting that these up-regulated DEGs likely regulate specific cell-cluster differentiation. Additionally, from these up-regulated DEGs, the top five genes from each cluster were selected to create a profile of 90 DEGs (Figure S3B). Among these, five TFs demonstrated the potential ability to regulate stem cell development due to their higher expression levels.

To determine the stem cell types, various cell clusters were annotated based on the previously reported specific marker gene in the stem cell spatial transcriptome. As a result, cluster 0 represented the cortex cell with markers *RD22* and *LOC112736871*, cluster 1 indicated the pith cell with *WRKY12*, clusters 7 and 11 were classified into epidermis/exodermis group with two highly expressed *MALD3* and *LOC112765980* and cluster 5, 9 and 14 were identified as xylem cell with *CSLG2*, *LOC112698114* and *LOC112794257*. Additionally, the xylem contained the cluster with *WAT1*, *MTI* and *LOC112744384* (Liu et al., 2022). The abundance of all marker genes was highly expressed and enriched in their corresponding cell types (Figure 1c). snRNA-seq mapped the transcriptome of peanut stems, establishing a foundational gene expression database to facilitate the exploration of transcriptional regulation mechanisms that govern stem cell ontology.

### Identification of DEGs and transcription factors interaction network in distinct stem cell types

To identify the DEGs in various cell types, original cell distribution map (18 clusters) was reanalysed with marker genes

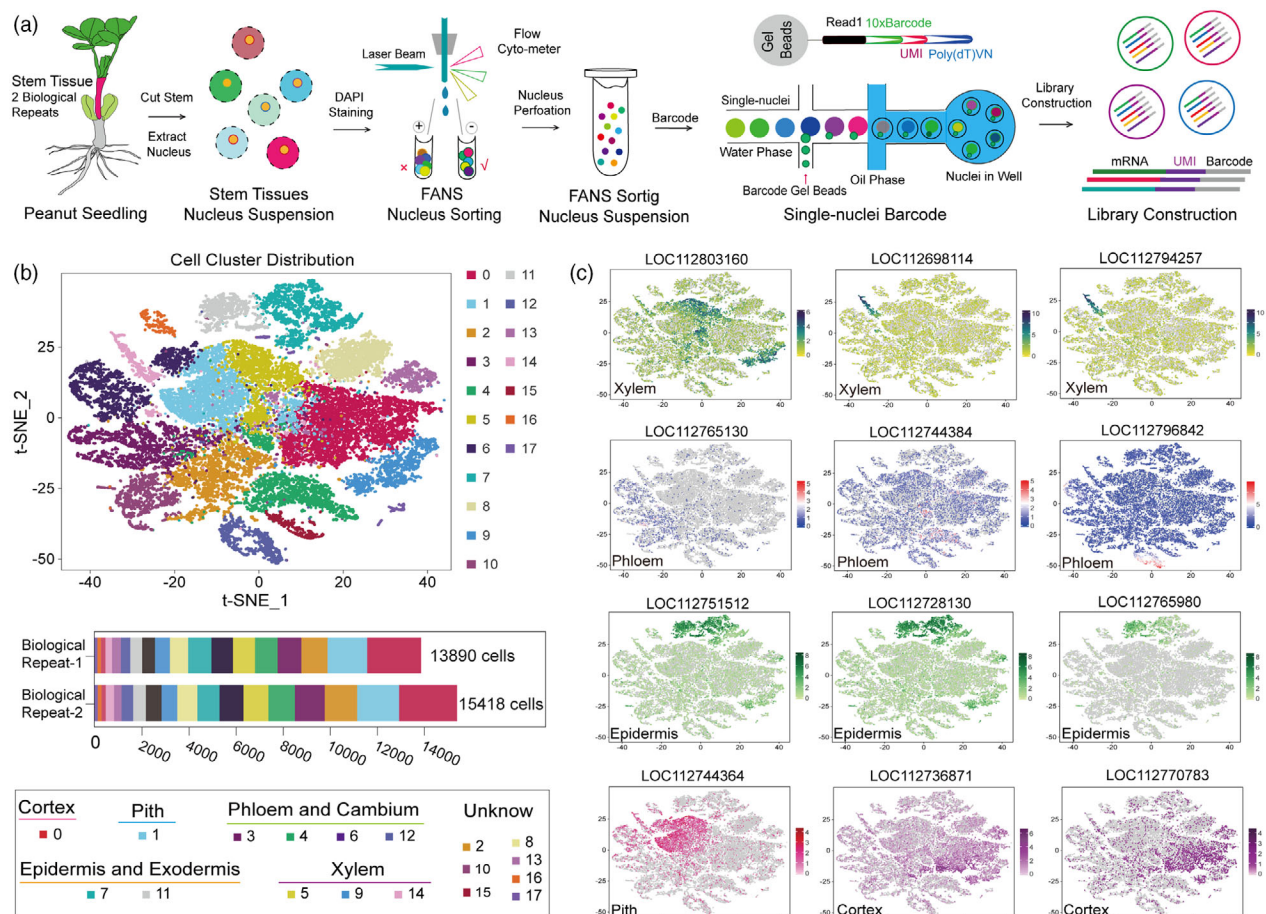


**Figure 1** Assembly of a single-cell transcriptome atlas in peanut stem cell based on single-nuclei RNA-seq (snRNA-seq): (a) Workflow of snRNA-seq experiment in peanut stem cell with FANS and microdroplets captured single nuclei to construct the sequencing library; (b) tSNE-map distribution displays the 18 cell clusters obtained by snRNA-seq in stem, each dot indicated a single-cell; (c) tSNE-map displays the marker genes expression distribution in cell clusters to identify the cell types.

for specific cell types after removing the unknown cell clusters. The new cell-distribution t-SNE map consisted of 22 319 individual cells (Table S2) classified into five cell types, including the epidermis/exodermis, phloem/cambium, cortex, pith and xylem (Figure 2a). Herein, we constructed a stem single-cell transcriptome profile with all identified expressed genes (Figure 2b). Furthermore, a total of 2053 up-regulated DEGs (Table S5) were identified across the five cell types ranging from 208 to 839. The highest number of 839 DEGs was found in the phloem cell, followed by 526 DEGs in cortex cells, 489 DEGs in epidermis group, 366 DEGs in pith cells and the lowest number of 208 DEGs in xylem cells (Figure 2c). Additionally, we found that distinct cell types are involved in diverse biological pathways (Figures S4, S5). For instance, glycan biosynthesis was observed in the cortex and pith, while phloem lacked DEGs associated with terpenoids and polyketides metabolism. These specific pathways likely influence the development of specific cell types.

Meanwhile, within this profile of up-regulated DEGs, the top five genes with the highest expression levels from each cell type were selected, resulting in a matrix of 23 DEGs. In the peanut stem bulk RNA-seq profile (Figure S6), 14 new marker genes were identified, with the majority showing up-regulation at the

day 7 growth time point by the quantitative real-time PCR. These DEGs can serve as new marker genes for identifying cell types in future stem single-cell experiments (Figure 2d). Additionally, we identified 85 critical TFs without duplication from the 2053 DEGs (Table S5). The majority of these differentially expressed TFs were involved in several important biological process (GO enrichment), such as regulation of DNA transcription, macromolecule biosynthesis, gene expression, nitrogen compound metabolic, response to stress and light stimulus (Figure 2e). Furthermore, KEGG analysis showed that 85 TFs mainly involved in the diterpenoid synthesis, aminoacids and nucleotide sugar metabolism, stilbenoid, diarylheptanoid and gingerol biosynthesis, and circadian rhythm pathways (Figure S7). This suggests that above-mentioned pathways likely regulate distinct cell-type development through transcriptional regulation in the stem. Among these TFs, 23 composed a core interaction network, providing a potential resource for further exploring their functions in the relationship between TFs and cell-type development in the stem (Figure 2e). Overall, the identifications of DEGs and TFs in stem cell extended our understanding of TF-induced transcription dynamic and specific biological pathways that influence distinct stem cell development.

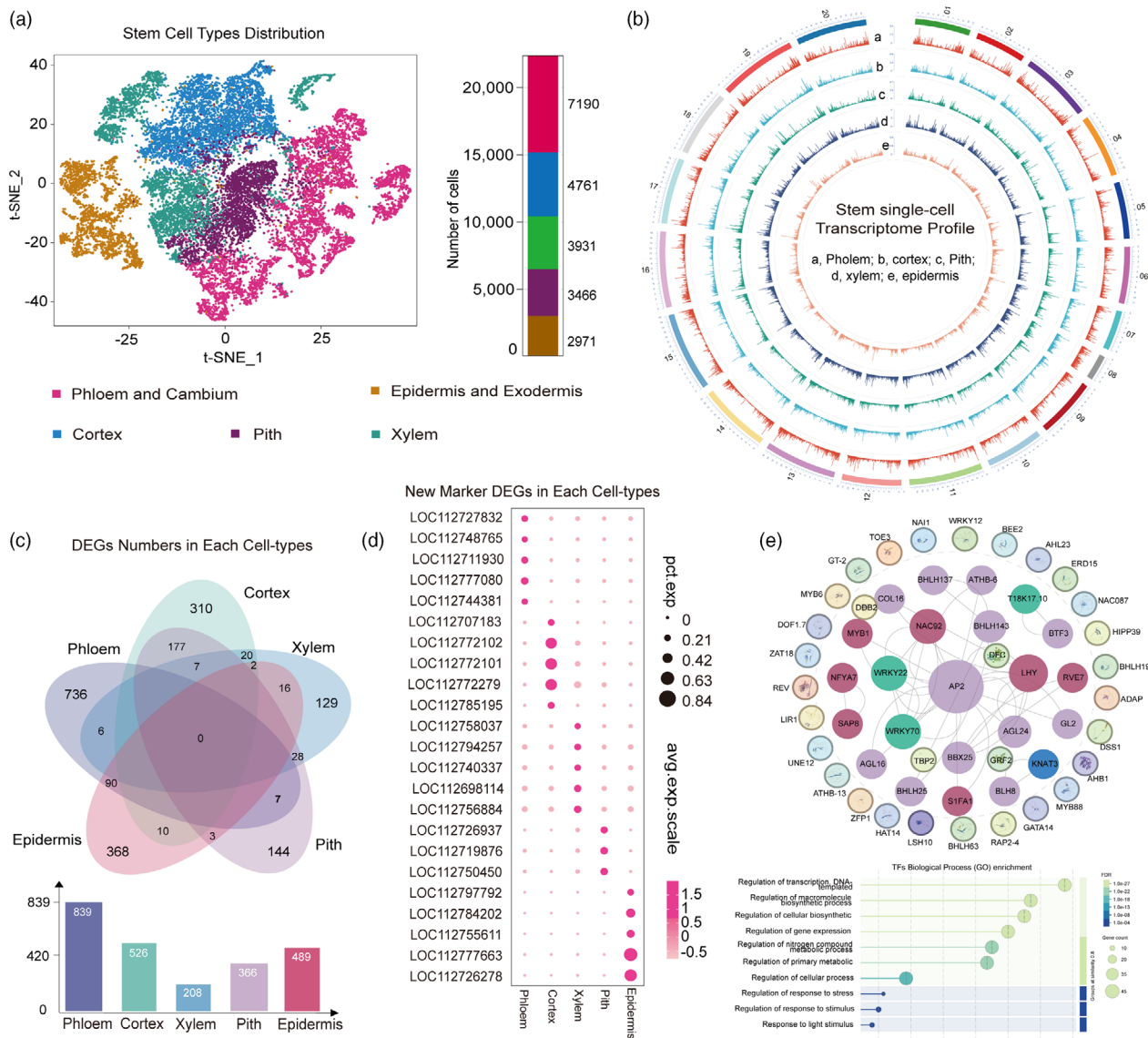


**Figure 2** Identification of DEGs and important TFs in stem cell types: (a) Re-united cell distribution map (t-SNE) of five cell types in stem; (b) Genes expression circle diagram of identified stem cell types. The outer circle indicates the 20 peanut genome chromosomes: (a) phloem; (b) cortex; (c) pith; (d) xylem; (e) epidermis; (c) Venn diagram represents the up-regulated DEGs distribution in different stem cell types; (d) New marker genes with higher expression level in each cell types, top five genes were selected as new marker genes form each stem cell types; (e) The interaction network of 23 TFs that respond to the stem cell-type development and TFs GO enrichment analysis. Solid line indicated the direct interaction relationship between different TFs, and circle-dotted line indicated the indirect interaction relationship.

#### Heterogeneity of transcriptional regulation in the developmental pathways of various stem cell types

Subsequently, to understand the stem cell development trajectory, the spatial and temporal distribution of DEGs expression driving cell differentiation in all stem cell types was investigated using pseudo-time analysis and partition-based graph abstraction (PAGA) model. The current analysis revealed that the stem cell developmental trajectory comprises two distinct branches, identified through the differential expression of 15 145 trajectory-specific genes (DEGs) along the primary pathway (Table S6). Five distinct cell-type differentiation states (Figure S8) were characterized, each marked by unique visual colour coding

based on the expression patterns of 21 287 DEGs (Table S7). Furthermore, 14 383 DEGs (Table S8) were determined to be critical indicating the fate of stem cell differentiation (Figure 3a). Moreover, the PAGA model identified 625 DEGs (Table S9) in distinct cell types, providing the correlation index between the five cell types. For example, the epidermis cells appeared to develop independently due to their low correlation index with other cell groups. In contrast, the cortex showed an intimate connection with the vascular groups (xylem, phloem, pith), indicating that they differentiate together (Figure 3b). We next filtered 3306 core DEGs from the cross-matching profile of pseudo-time and PAGA analysis, among which 147 TFs (Figure 3c) exhibited potential transcriptional regulation abilities that influence the stem cell

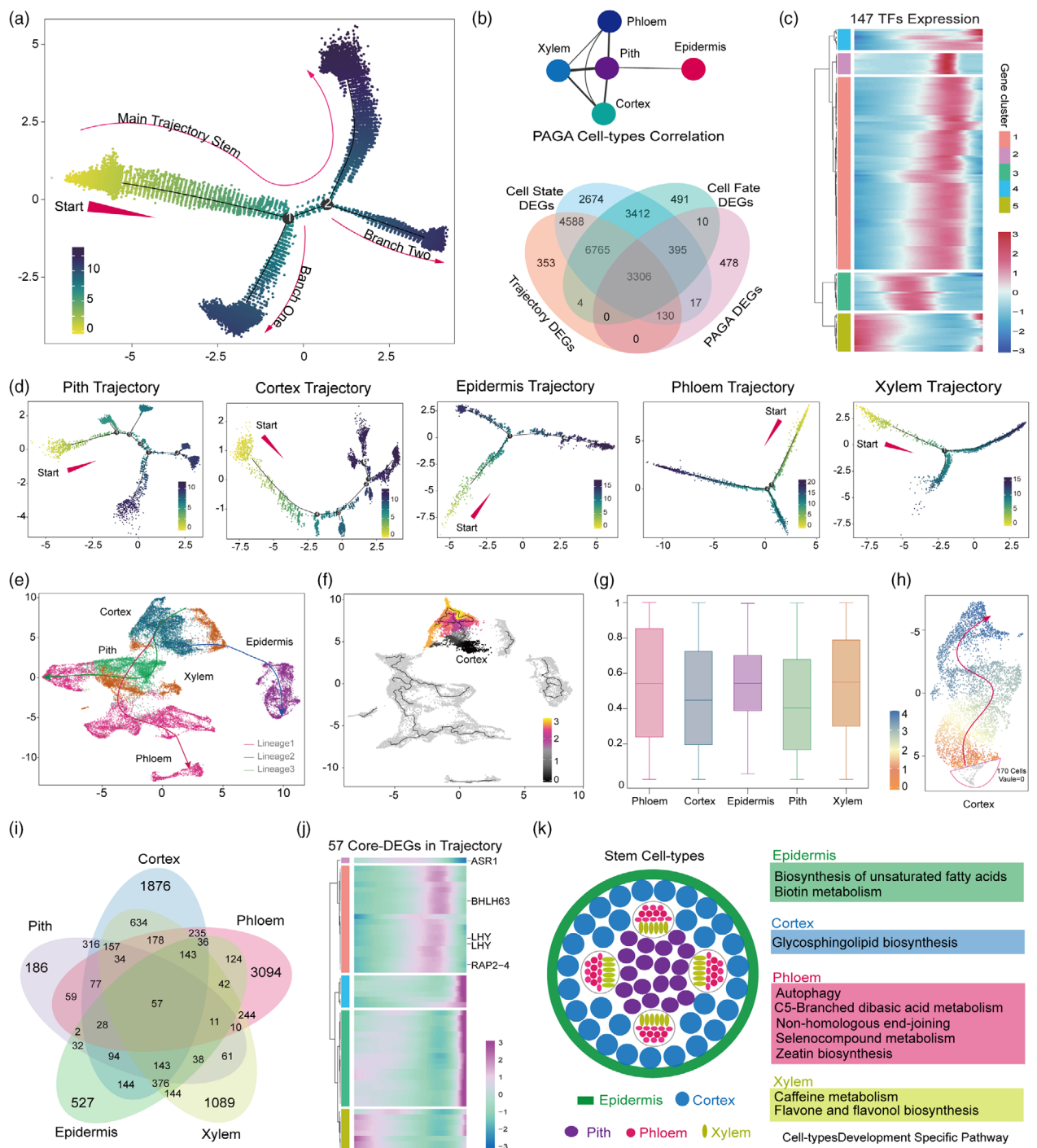


**Figure 3** Comprehensive analysis of stem cell development trajectory: (a) Development trajectory of identified stem cells using the pseudo-time analysis; (b) The correlation between different cell types in stem calculated via PAGA model along with a Venn diagram highlighting the core-DEGs by cross-matching pseudo-time and PAGA analysis; (c) Expression trends of 147 transcription factors (TFs) across the stem cell development trajectory; (d) Differentiation trajectories of distinct cell types in the stem; (e) Slingshot predicted cell development lineage of distinct cell types; (f) Monocle 3-predicted development trajectory of all identified stem cells; (g) Cytotrace computed differentiation values of different cell types; (h) Slingshot inferred putative development lineage of stem cortex cell; (i) Venn diagram displaying specific DEGs by cross-matching the pseudo-time analysis of distinct stem cell types; (j) Expression trends of 57 core DEGs in the cell differentiation trajectory; (k) Specific biological pathways associated with the development trajectories of distinct cell types.

development trajectory. The majority of these TFs were found to be involved in plant-pathogen interaction and hormone signalling transduction.

To elucidate the distinct developmental characteristics of various cell types, pseudo-time analysis was employed on five independent cell populations. In cortical cells, a total of 3931 cells

delineated a developmental trajectory encompassing six branch nodes and 4528 DEGs associated with the trajectory. Pith cells, consisting of 3466 cells, exhibited a developmental path with five branch nodes and 1305 trajectory DEGs. Epidermal cells demonstrated a simpler structure with one branch node and 1941 trajectory DEGs. Phloem cells, comprising 7190 cells, revealed a developmental trajectory with two branch nodes and 4374 trajectory DEGs. Lastly, xylem cells, with a total of 3361 cells, were characterized by one branch node and 3361 trajectory DEGs (Figure 3d). These findings indicate that cortical and pith cells exhibit higher differentiation activity and cellular polymorphism, as evidenced by their greater number of branch nodes in their cell differentiation state (Figure S9). To delineate the developmental lineage relationships among different cell types, the Slingshot algorithm was utilized, revealing three distinct cell lineages in the reflected cell distribution map. Lineage 1 comprised the cortex, xylem and phloem pathways; lineage 3 included the cortex, pith and phloem; while epidermal development appeared to be independent, as indicated by lineage 2 (Figure 3e). This suggests that cortical cells develop earlier than other cell types, a conclusion supported by the Monocle 3-predicted cell trajectory map (Figure 3f). However, Cytotrace evaluation showed that cortical cells had a lower differentiation value compared to other cell types, with epidermal cells exhibiting the highest differentiation value due to their unique developmental pathway (lineage 2) (Figure 3g). Additionally, re-computation with Slingshot inference identified 170 isolated cortical cells that did not participate in any lineage events (Figure 3h). Overall, the cell trajectory analysis provided a comprehensive understanding of the developmental and differentiation relationships among cell types during stem growth. Furthermore, cross-matching analysis showed that the 57 co-DEGs were present in the development trajectory DEGs profiles of all cell types (Table S10), exhibiting differential expression levels. These co-DEGs might be the conserved genes that promote the cell types differentiation. Additionally, there were 186, 1876, 3094, 1089 and 527 specific DEGs appeared in pith, cortex, phloem, xylem and epidermis, respectively (Figure 3i,j). Upon sorting the specific DEGs to identify their associated biological pathways, it was found that glycosphingolipid biosynthesis specifically regulates cortex differentiation. In phloem cells, five distinct pathways were identified: autophagy, C5-branched dibasic acid metabolism, non-homologous end-joining, seleno-compound metabolism and zeatin biosynthesis. This suggests that the cytokinin phytohormone zeatin is crucial for phloem development. Xylem differentiation was critically influenced by caffeine metabolism and flavone biosynthesis. In epidermal cells, the biosynthesis of unsaturated fatty acids and biotin metabolism was specifically involved, likely because wax and cutin biosynthesis on the stem surface require fatty acids. Additionally, no specific biological pathway was identified in the pith development trajectory, implying that pith development follows general biological pathways similar to other cell types (Figure 3k).

#### Stem bulk RNA-seq identifies the DEGs in transcriptome profiles at distinct time-point

Although snRNA-seq provides detailed profiles of DEGs and key TFs at single-cell resolution in stem tissues, it remains unclear if these critical TFs maintain high expression levels at the tissue level during stem development. To address this, bulk RNA sequencing (RNA-seq) was conducted to map the transcriptome of stems at different developmental stages (Table S11), specifically at early

development (3 days) and rapid elongation (7 days). This analysis identified 10 810 DEGs (Table S12), of which 6703 upregulated and 4107 downregulated at 7 days compared to 3 days (Figure 4a,b). The genes identified at both time points were mapped onto the cultivated peanut chromosomes, creating a comprehensive bulk RNA-seq transcriptome landscape of the stem (Figure 4c). By comparing cell types identified by snRNA-seq with DEGs from bulk RNA-seq, 763 core DEGs (Table S13) were found to exhibit differential expression across various cell types and developmental stages. Of these, 297 core DEGs were upregulated and 466 were downregulated (Figure 4d). These core DEGs were predominantly involved in pathways such as ribosome biogenesis, ketone body synthesis, terpenoid biosynthesis, glyoxylate cycle and flavonoid biosynthesis (Figure 4e). Furthermore, 31 TFs were identified among the 763 core DEGs, indicating that these core TFs not only regulate cell type-specific differentiation (e.g., cortex and epidermis) but also influence stem growth at different stages by modulating pathways related to phytohormone signalling, pathogen resistance and circadian rhythms (Figure 4f), further quantitative real-time PCR was conducted to validate the expression levels of 12 TFs (Figure S10). The results indicated that the expression trends of these key TFs were consistent with the bulk transcriptome data.

Additionally, by comparing trajectory DEGs with bulk RNA-seq DEGs, we identified 3019 core DEGs (Figure 4g). Within these, 334 TFs were found to significantly impact stem cell differentiation across various growth stages by mediating hormone signalling pathways. A comparison with the *Arabidopsis* genome revealed homologous genes, leading to the construction of a TF interaction network centred around 60 TFs, with WRKY, BHLH and PIF proteins at the core (Figure 4h). This network underscores the pivotal role of these TFs in stem elongation. Furthermore, integrating DEGs from snRNA-seq, bulk RNA-seq and trajectory analyses revealed 27 core TFs that synchronously mediate stem cell development, differentiation and elongation at single-cell resolution and across different stages of growth (Figure 4i). These findings offer a crucial resource for future studies aiming to validate the role of TFs in regulating stem growth.

#### Identification of cell cycle core-DEGs during the stem development

During stem cell development, the phases of the cell cycle manifest distinct transcriptional characteristics. Utilizing established cell cycle marker genes, we assessed the cell cycle phase of identified stem cells. Our findings revealed a predominance of stem cells in the S phase compared to other phases, while G1 and G2/M phases collectively encompassed more cells than M, G1/S and non-cycling (NC) phases (Figure 5a,b; Figure S11). Subsequent analysis of DEGs across these phases identified 740 DEGs specific to the S phase (Figure 5c), contrasting with only 6 DEGs identified in the M phase. This underscores a correlation between gene expression profiles and the S, G2/M (368 DEGs) and G1/S (443 DEGs) cell cycle phases. Despite the limited number of cells in the NC phase, 502 DEGs were identified, suggesting that NC-associated DEGs modulate specific pathways influencing cellular heterogeneity. To further characterize these phases, we identified 30 new top DEGs per cell cycle phase for future differentiation of stem cell states using snRNA-seq (Figure 5d).

To elucidate the biological roles of 1445 cell cycle DEGs (Table S14), we integrated snRNA-seq identified DEGs across cell types, bulk RNA-seq identified DEGs from various stem growth time points and cell cycle DEG profiles to identify core DEGs. This

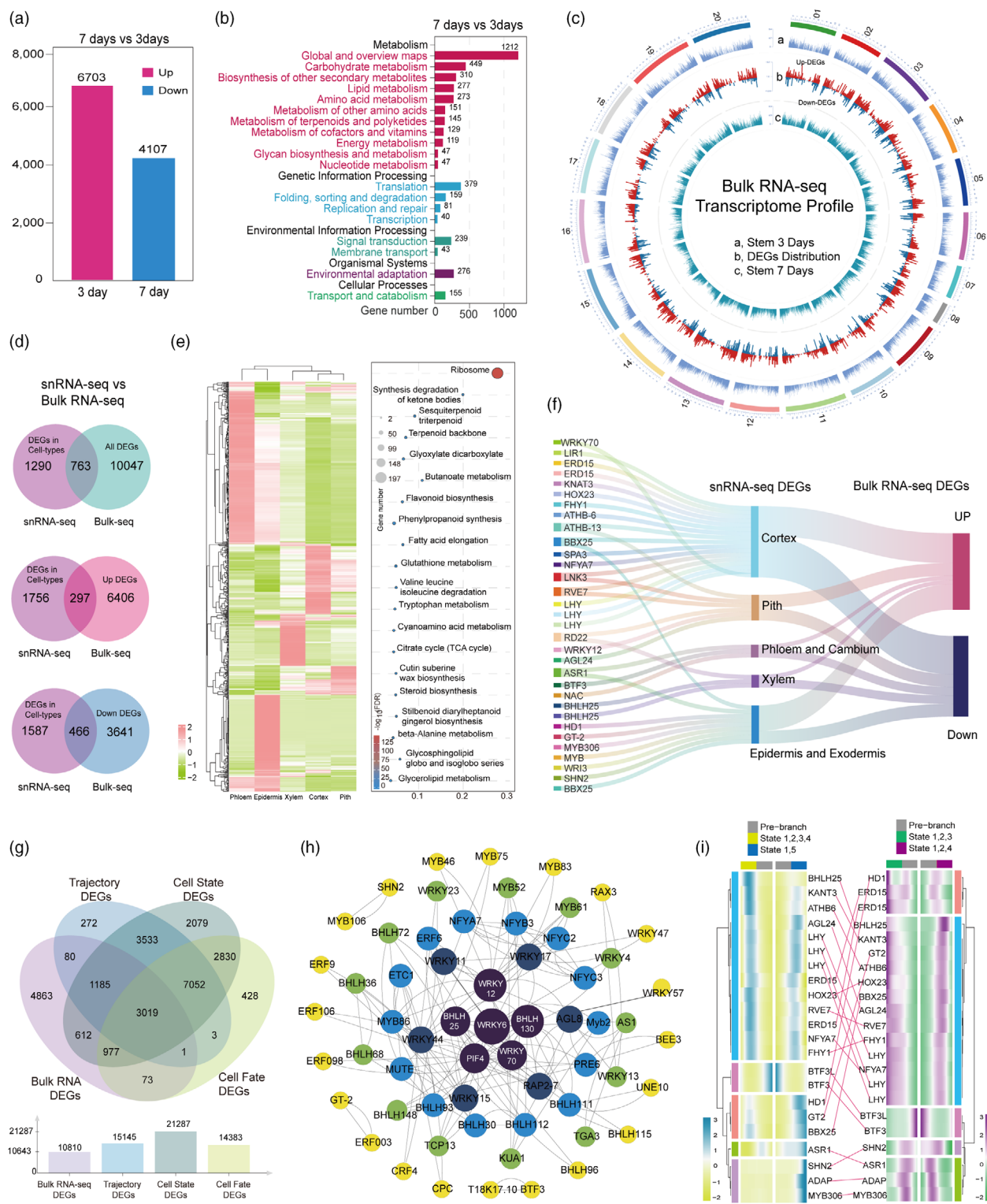


**Figure 4** Integration of snRNA-seq and bulk RNA-seq for the identification of transcription factors interaction network in peanut stem: (a) Histogram displaying the DEGs at distinct time-points of stem growth, early stage (3rd day) and elongated stage (7th day); (b) Identification of DEGs involved in top KEGG pathways via Bulk RNA-seq; (c) A comprehensive transcriptome atlas of peanut seedling stems grown at different time points, visualized from outer to inner circular layers: (a) representation of all expressed genes in the 3-day-old stem tissue; (b) distribution of differentially expressed genes (DEGs) across the stem tissue; (c) depiction of all expressed genes in the 7-day-old stem tissue; (d) identification of 763 co-existed DEGs in snRNA-seq and bulk RNA-seq DEGs profiles; (e) 763 co-existed DEGs expression matrix and respond metabolism pathway in stem cell types; (f) Sankey diagram shown the critical TFs expression tendency between the stem cell types and tissue level; (g) Identification of core-DEGs in bulk RNA-seq and cell trajectory DEGs profiles; (h) Interaction regulation network of 60 TFs that filtered from the 3019 core-DEGs; (i) 22 TFs expression pattern at the branch nodes 1 and 2 of all identified cells differentiation trajectory.

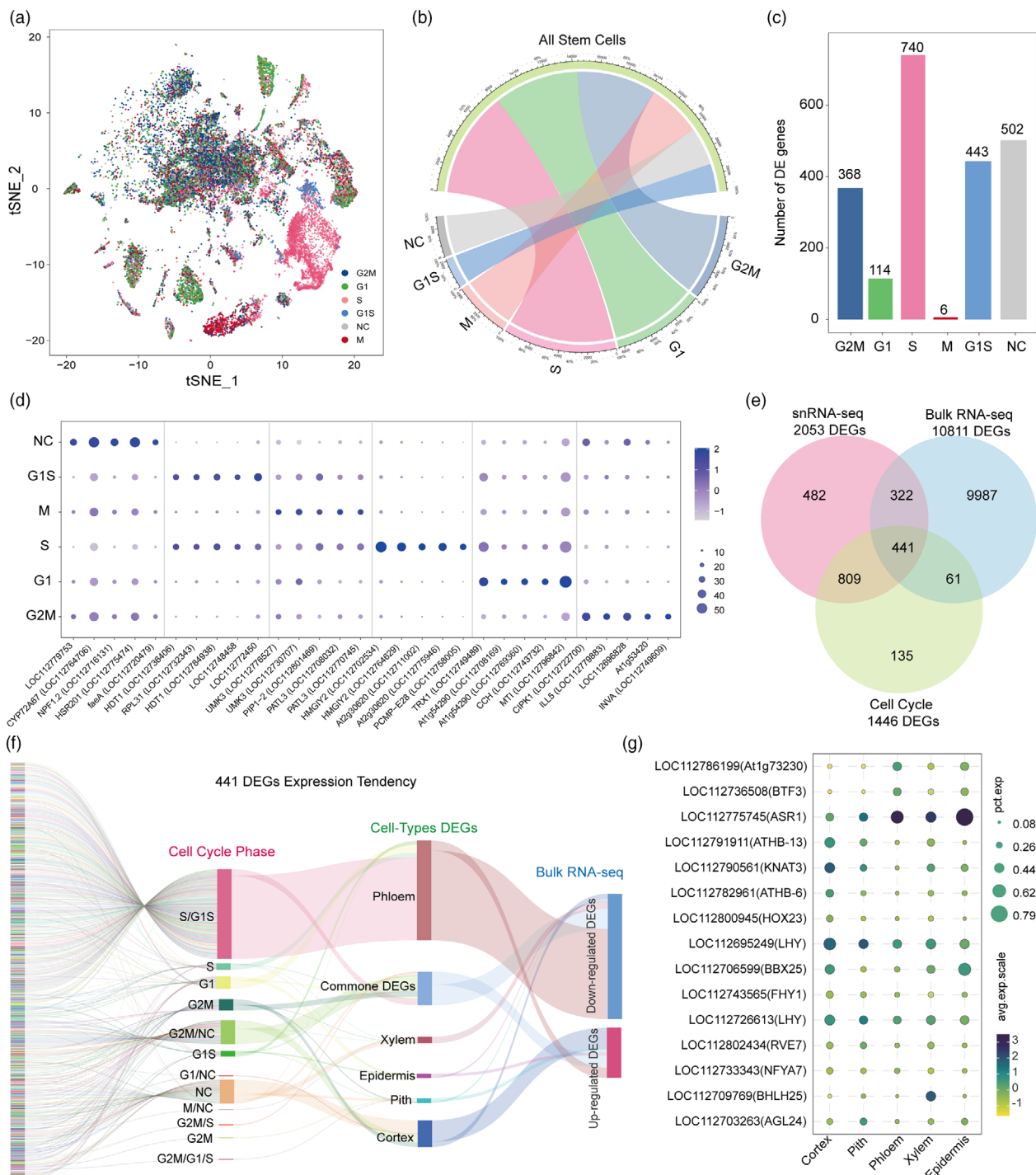


**Figure 5** Integration of cell types, cell cycle and bulk RNA-seq to identify the core-DEGs and important TFs: (a) Cell cycle state distribution of total stem cells in tSNE map; (b) Cell cycle phase distribution, NC indicates the non-cycling cell population; (c) Histogram plot displaying the DEGs in different cell cycling phase; (d) New identified marker genes for distinguishing stem cell genome replication states; (e) Venn diagram shows 441 core-DEGs between cell cycling DEGs, snRNA-seq identified cell-type DEGs and bulk RNA-seq identified DEGs in distinct stem growth time-point; (f) Expression dynamics of 441 DEGs in cell-cycle, cell-type and bulk RNA-seq profiles; (g) Expression levels of 15 core-TFs in different cell types.

integration yielded a total of 441 DEGs (Figure 5e), including 251 DEGs down-regulated in the S/G1S phases of phloem and 34 DEGs up-regulated in the NC phase of cortex cells (Figure 5f). Further filtering identified 15 differentially expressed core TFs from the 441 DEG profile, with a predominant representation in

the NC DEGs profile, influencing cell type ontology and differentiation (Figure 5g). Our study of cell cycle DEGs provides a resource for future investigations into the role of individual genes in regulating stem cell differentiation, cell cycle dynamics and temporal elongation processes.

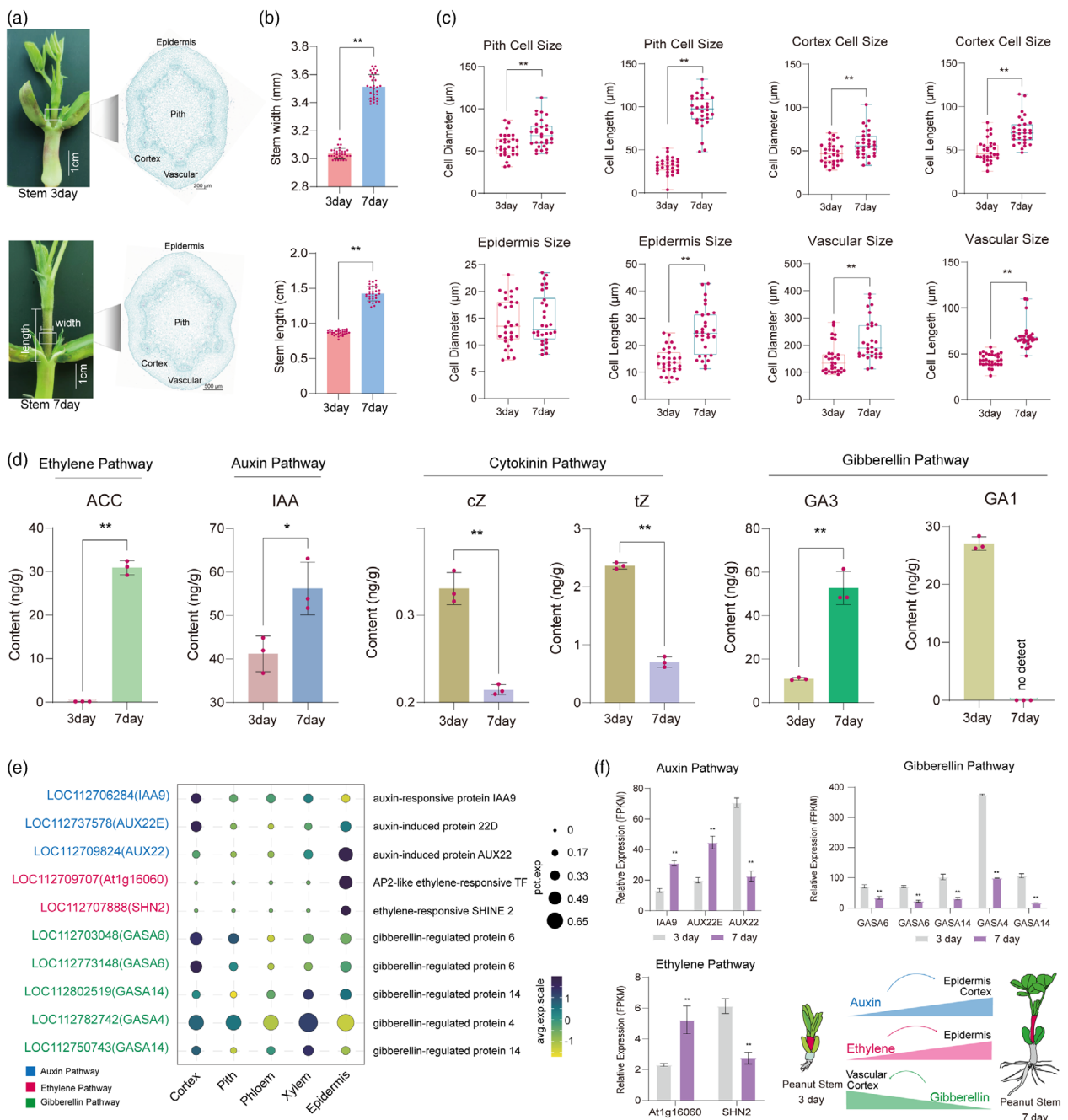


**Figure 6** Plant growth hormones correlated with the peanut stem development: (a) Phenotype and transverse section of peanut stem at early stage (day 3) and elongated stage (day 7); (b) Investigation of peanut seedling stem width and length at days 3 and 7 ( $n = 30$ ); (c) Investigation of stem cell (pith, cortex, epidermis and vascular) size by observing the transverse section at days 3 and 7 ( $n = 30$ ); (d) Plant growth hormones examination in peanut seedling stem at days 3 and 7 with three biological repeats; (e) Identification of hormone respond genes expression at single-cell resolution from 736 DEGs profile (Figure 4d) in distinct peanut stem cell types; (f) Hormone respond genes relative expression with tissue level at different growth time-point (days 3–7), and a putative model to describe the hormone regulated cell-type development in peanut seedling stem. All statistical significance was indicated as \* $P < 0.05$  and \*\* $P < 0.01$  ( $t$ -test).

#### Plant hormone pathways are tightly correlated with stem growth

Peanut seedling stems initially elongate at early stages (3 day) after emerging from soil, and the first internode stretched completely by 7th day (Figure 6a). The stem width (diameter)

and length were significantly larger at 7th day as compared with the 3rd day (Figure 6b). To understand which cell types were most relevant to hormone increase during the stem growth, we calculated cells sizes at different growth time points by analysing the histologic sections. Observations of stem transverse sections suggested that the cell sizes of pith, cortex and vascular tissues

were larger at 7th day than at 3rd day. However, the larger cortex and pith cell sizes resulted in fewer cells per unit area at 7th day. Additionally, the epidermis diameter did not change significantly, but epidermis length increased from day 3 to day 7 (Figure 6c). These observations indicate that the cortex and pith cells contributed most to an increase in the stem thickness and length.

Integrating snRNA-seq with bulk RNA-seq leads to the identification of several TFs involved in hormone signalling transduction pathway, suggesting that hormones may regulate the stem development. Additionally, stem tissue gradually elongates against gravity after the seedling emerges from soil, with multiple phytohormones playing important roles in controlling this elongation process. To understand the hormone content variations at different stem growth stages, we examined six types of phytohormones and their chemical derivatives (Table S15). The analysis revealed a marked increase in the ethylene biosynthesis precursor aminocyclopropane carboxylic acid (ACC) and the auxin biosynthesis compound indoleacetic acid (IAA) from day 3 to day 7. Moreover, there was a significant rise in the levels of auxin derivatives, such as indole-3-acetyl glutamic acid (IAA-Glu), indole and indole-3-carboxaldehyde at day 7. In contrast, the concentrations of cytokinins, including *cis*-zeatin (cZ) and *trans*-zeatin (tZ), notably decreased at day 7. In the gibberellin pathway, gibberellic acid (GA3) content increased at day 7, while GA1 was only detected at day 3 and did not follow the same trend as GA3 (Figure 6d). These observations suggest that auxin plays a crucial role in stem development, with the SAM regulating sustained stem growth, a vital process for promoting stem cell proliferation.

Furthermore, we identified ten hormone-responsive genes that were present in both the cell-type-specific and bulk DEG profiles (Figure 4d, 736 DEGs). These included three auxin-responsive genes (*IAA9*, *AUX22E*, *AUX22*), two ethylene-responsive TFs (*AP2*, *SHN2*) and five gibberellin-regulated genes (*GASA4*, *GASA6*, *GASA14*). *IAA9* and *AUX22E* showed high enrichment in the cortex and were up-regulated at 7 days, indicating their role in the auxin pathway to promote stem growth by influencing cortex enlargement. The ethylene-responsive TFs were enriched in the epidermis, contributing to increased epidermal cell length (Figure 6e). The five *GASA* genes were collectively down-regulated at 7 days at the tissue level (Figure 6f), which suggests that the down-regulation of GA1 is likely due to the reduced expression of *GASA* genes. In conclusion, we detailed the phytohormone dynamics associated with stem cell development and identified several potential hormone-responsive genes that regulate stem growth.

#### Peanut *AhWRKY70* protein feature and gene expression pattern

The integration of snRNA-seq and bulk RNA-seq enabled the identification of WRKY TFs enriched in differential expression genes (DEGs) profiles, encompassing both trajectory DEGs and those identified through single-nucleus and bulk RNA-seq methodologies. The *AhWRKY70* served as a core factor in the TF interaction network (Figure 2e), showing significant differential expression across snRNA-seq cell types (Table S5), bulk RNA-seq (Table S12) and stem development trajectory DEGs profiles (Tables S6–S8), these results suggest that *AhWRKY70* likely influences the peanut stem growth. Therefore, we subsequently cloned the *WRKY70* TF from the peanut stem and validated its molecular function. The coding sequence of *AhWRKY70* (GenBank: LOC112797210) spans 921 base pairs, translating into a protein of 306 amino acids. Structural analysis revealed two

conserved domains within the *AhWRKY70* protein: a SCOP domain located between residues 16 and 72 and a WRKY DNA-binding domain located between residues 127 and 189 (Figure 7a). These findings suggest that the *AhWRKY70* TF binds to specific DNA motifs, thereby regulating the expression of downstream target genes. Phylogenetic analysis further demonstrated significant homology between *AhWRKY70* and *Arabidopsis WRKY22* (Zhou et al., 2011) (Figure 7b), leading us to speculate that *AhWRKY70* may have a similar function to *WRKY22*. Current results confirmed that *AhWRKY70* protein is located in the nucleus (Figure 7c). *AhWRKY70* expression was highly enriched in the cortex and xylem at single-cell resolution (Figure 7d) and significantly regulated cell fate differentiation with different expression patterns at the branch node 2 in the overall cell development trajectory (Figure 7e). Furthermore, we detected *AhWRKY70* expression in a previously generated leaf cell-type atlas, which indicated that *AhWRKY70* was highly expressed in the vascular cells (bundle sheath and xylem) (Figure 7f). Additionally, the quantitative real-time PCR results indicated that the relative expression level of *AhWRKY70* was consistent with the tissues transcriptome data (Figure S12). These results suggest that *AhWRKY70* may play a role in the regulation of leaf vascular development.

Based on our unpublished peanut tissue transcriptome atlas (unpublished), *AhWRKY7* expression was significantly up-regulated in the early stem tissue (3 days) when compared to 7-day-old stem (Figure 7g). This result indicates that *AhWRKY70* tissue expression pattern has a positive correlation with stem growth rate. However, the expression of *AhWRKY70* during the seed development from day 5 to day 45 (Figure 7h) implies that *AhWRKY70* likely does not modulate the peanut seed growth. *AhWRKY70* expression did not show significant differences among various tissues (leaf, hypocotyl, root, lateral root) of one-week-old peanut seedling but was significantly elevated in flowers, aerial pegs, subterranean pegs and fruit pods (Figure 7i), suggesting that *AhWRKY70* may play a role in regulating peg and pod development at the reproductive stage. In leaves exposed to different light conditions, *AhWRKY70* expression was higher under dark growth condition (Figure 7j). *AhWRKY70* expression patterns in different flower tissues showed higher expression levels in sepals, calyx tubes and styles (Figure 7k), demonstrating that *AhWRKY70* exhibits tissue-specific expression and potential multi-functionality at both tissue and single-cell resolutions.

Moreover, we analysed the *AhWRKY70* promoter haplotypes based on a collection of previously re-sequenced 390 peanut accessions (Lu et al., 2024). In the promoter region of *AhWRKY70*, two mutant sites were identified at –1272 bp (G/A) and –1888 bp (T/C) upstream of the start codon (ATG) (Figure 7l). A reduced plant height (main stem height) was observed in case of haplotype 1 (G/C) as compared to haplotype 2 (G/T) and 3 (A/T) plants (Figure 7m). Further examination of *AhWRKY70* expression in different peanut accessions (30 independent germplasm resources) before flowering period showed that the haplotype 1 significantly repressed *AhWRKY70* expression levels (Figure 7n). Using the PlantPAN 4.0 web tool (Chow et al., 2024) we analysed the conserved DNA-motif in *AhWRKY70* promoter sequence (Figure S13). This analysis identified six conserved DNA-binding motifs at position –1272 bp with the sequence of GCCAT (G-type). However, a mutation in the *AhWRKY70* promoter sequence changed this site from G to A, introducing additional potential TF binding sites at position –1272 bp (A-type, TGTCGTCATT), including bZIP/B3

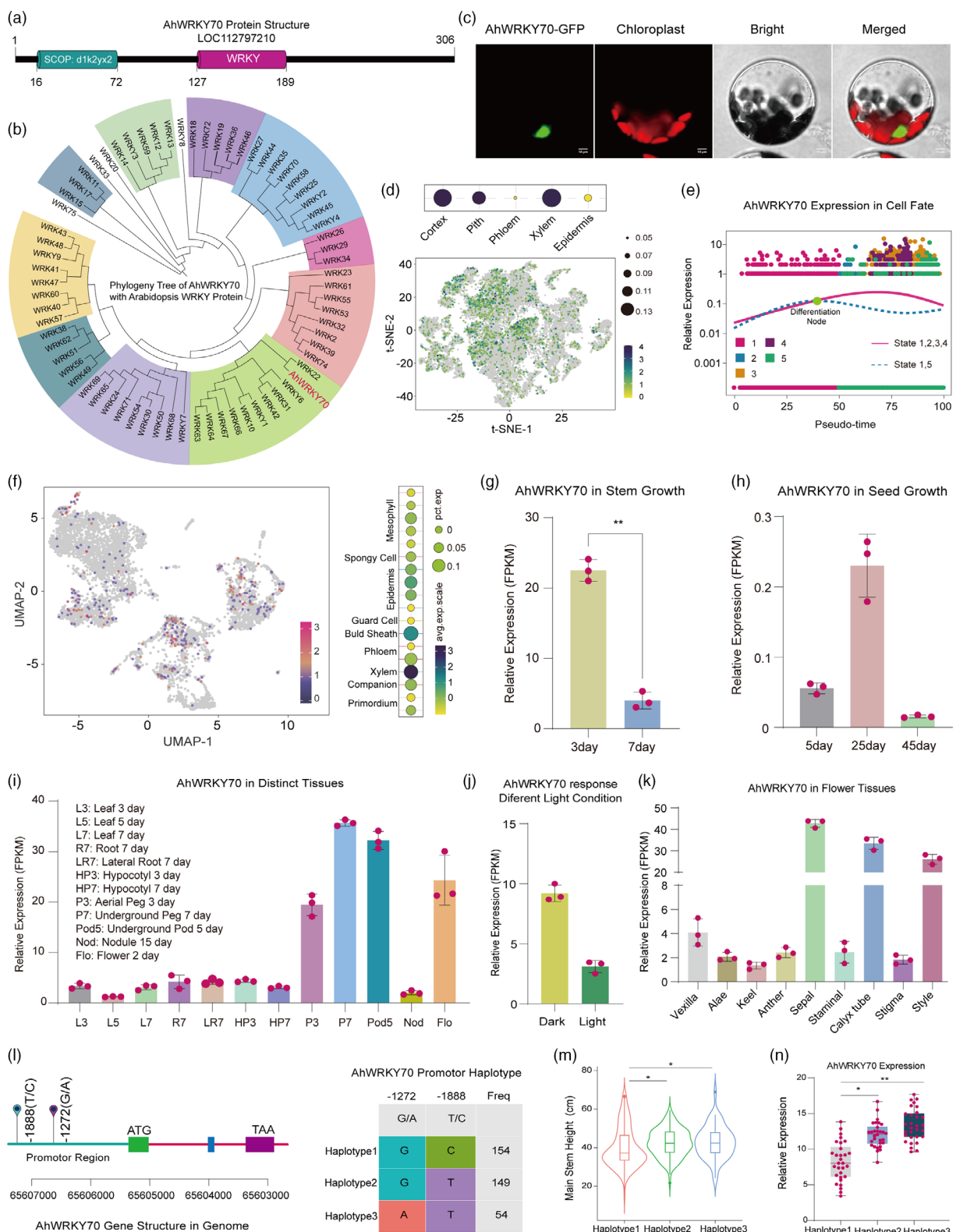


**Figure 7** Peanut AhWRKY70 protein characteristics and expression patterns: (a) Conserved domain analysis in peanut AhWRKY70 protein structure, SCOP domain (16–72 aa) and WRKY domain (127–189 aa); (b) Phylogenetic analysis of AhWRKY70 and 69 *Arabidopsis* WRKY genes; (c) Subcellular localization of AhWRKY70 protein in *Arabidopsis* protoplast cell; (d) Expression dynamics of AhWRKY70 in different stem cell types; (e) AhWRKY70 expression tendency modulated the cell development trajectory; (f) The expression level of AhWRKY70 in leaf single-nucleus RNA-seq profile; (g–k) AhWRKY70 expression pattern in stem growth at 3 and 7 days (g), seed development (h), distinct tissues (i), leaf respond light and dark growth condition (j) and dissected flower tissue (k); (l) AhWRKY70 promoter haplotype mutant site; (m) haplotypes of AhWRKY70 promoter in 390 peanut accessions; (n) AhWRKY70 haplotypes expression levels in different peanut accessions ( $n = 30$ ). All statistical significance was indicated as  $*P < 0.05$  and  $**P < 0.01$  ( $t$ -test).

TFs, homeodomain TFs and TGA-box binding factor (Table S16). These findings suggest that the binding motif at  $-1272$  bp may play a crucial role in regulating *AhWRKY70* expression. Meanwhile, the distinct promoter haplotypes affected *AhWRKY70* expression. Furthermore, distinct promoter haplotypes impacted *AhWRKY70* expression levels, with higher expression associated with increased plant height in peanuts.

#### *AhWRKY70* regulates plant stem cell development through hormonal signalling

To illustrate the molecular mechanism by which *AhWRKY70* regulates the stem growth, we ectopically overexpressed *AhWRKY70* in *Arabidopsis* and obtained positive *AhWRKY70-OE* transgenic plants (Figure 8a; Figure S14). The *AhWRKY-OE* lines exhibited accelerated growth compared to wild-type plants, with earlier entry into the bolting stage, signalling the commencement of stem development (Figure 8b). The stem length was notably greater in the *AhWRKY70-OE* lines relative to the wild-type plants (Figure 8c). Additionally, other fundamental morphological indicators of stem growth, such as earlier branch elongation and reduced flowering time, showed significant differences in *AhWRKY70-OE* lines compared to wild-type plants (Figure 8d). These findings suggest that the overexpression of *AhWRKY70* promotes stem growth.

To further explore the mechanism by which *AhWRKY70* influences growth characteristics, we analysed the endogenous hormone content (Table S17) in *AhWRKY70* overexpression lines. Phytohormone assays revealed that the levels of IAA (auxin) and the ethylene precursor ACC were significantly elevated in the *AhWRKY70-OE* lines (Figure 8e). The up-regulation of auxin derivatives in *AhWRKY70-OE* lines suggests that *AhWRKY70* participates in auxin and ethylene signalling pathways to enhance stem growth in transgenic plants.

Furthermore, transverse sections of the stem during the complete elongation of the first internode were examined in both *AhWRKY70-OE* and wild-type plants grown under identical conditions (Figure S15). Observations indicated that the cell sizes of the stem cortex and epidermis were larger in overexpressed lines as compared to wild-type plants (Figure 8f), while other cell types remained unaffected (Figure S16). This implies that *AhWRKY70* promotes stem cortex and epidermis cell development through hormone pathway responses. Subsequently, transcriptome analysis via bulk RNA-seq was performed to identify the DEGs between *AhWRKY70-OE* and wild-type lines. A total of 1128 and 1233 DEGs (Table S18) were identified in the two *AhWRKY70-OE* lines compared to wild-type plants, respectively (Figure 8g). Among these, 679 co-DEGs (Table S19) were consistently expressed across both profiles (WT vs OE1, WT vs OE2), without significant differences in their expression trends. The majority of DEGs were associated with MAPK signalling, plant-pathogen interaction, hormone signalling and secondary metabolites pathways (Figure 8h). Notably, eight DEGs responsive to the auxin biosynthesis pathway were up-regulated in the *AhWRKY70-OE* lines, including two auxin synthesis regulators *YUCCA 8/9* and six auxin responsive genes (Figure 8i). Additionally, eight ethylene responsive factor encoding genes were identified, with only *EDF3* being up-regulated while the other seven *ERF* genes were down-regulated in the *AhWRKY70-OE* lines (Figure 8j). These findings indicate that *AhWRKY70* modulates the ethylene pathway by regulating the expression of ethylene-responsive factors. In conclusion, we proposed a model in which *AhWRKY70* regulates stem development through

the auxin and ethylene signalling pathways (Figure 8k). This study enhances our understanding of the potential roles of WRKY family TFs in the development of peanut tissue.

## Discussion

The plant stem is a crucial aerial part that supports upright growth (Peng et al., 2024). It connects various parts of the plant and transports nutrients and signalling molecules, essential for long-distance communication that impacts crop yields (Liu et al., 2021b; Ye et al., 2020). Stems also play a role in carbon storage and remobilization, influencing plant development (Furze et al., 2018). Despite its importance, most studies on peanut stems focus on stem rot (Korangi et al., 2023; Li et al., 2023b; Yan et al., 2023), with limited research on stem development regulation (Serrano-Mislata and Sablowski, 2018; Yu et al., 2022).

The peanut stem offers structural support and serves as an anchor for leaves, optimizing sunlight capture for photosynthesis. From the shoot node, lateral branches extend, lateral buds differentiate into flower buds and aerial pegs grow towards the soil. Stem height is a critical agronomic trait that shapes plant architecture and influences crop yield. Additionally, the angle at which the stem contacts the ground is a key determinant of pod number, a vital trait in peanut variety breeding.

From morphological observations to the cellular level, limited biological insights are available to explain the developmental mechanisms in peanut stem cells. To address this gap, snRNA-seq was performed to explore cell heterogeneity in 29 308 stem cells, using FANS and microfluidics methodologies to capture single nuclei. The establishment of the stem cell atlas provides a valuable gene resource for illustrating the functions of critical factors controlling stem cell-type ontology and differentiation. Our study significantly expands the understanding of stem development at single-cell resolution.

#### Peanut stem development correlates with the phytohormone signalling

Peanut architecture has three different types, with ancestral species having main stem and lateral branches that grow horizontally on the ground surface. Cultivated peanuts include the Spanish type with an up-regulated stem and branches (V-type) and Runner type with a rambling branches (U-type), both of which have undergone artificial selection. Although the draft genome and tissue transcriptome information of cultivated peanut have been released, the molecular regulation mechanisms of distinct-type stem development at single-cell resolution remain largely unknown. Herein, we employed snRNA-seq to describe the transcriptome atlas in single peanut stem cell (Spanish type), and stem bulk RNA-seq was carried out to identify the DEGs profile at different growth time-points. The integration of snRNA-seq and bulk RNA-seq has elucidated the complex TF interactions driving the transcriptional dynamics involved in stem cell differentiation. This approach has provided insights into the manipulation of various biological processes, including phytohormone signalling, circadian rhythms and environmental stress responses.

Stem growth is regulated by multiple phytohormone pathways, notably gibberellin (GA), brassinolide (BR) and strigolactone (SL). These pathways modulate the expression of a series of critical genes that control stem-induced plant height. For instance, genes such as *SD1* (Asano et al., 2011), *OsDWARF4* (Sakamoto

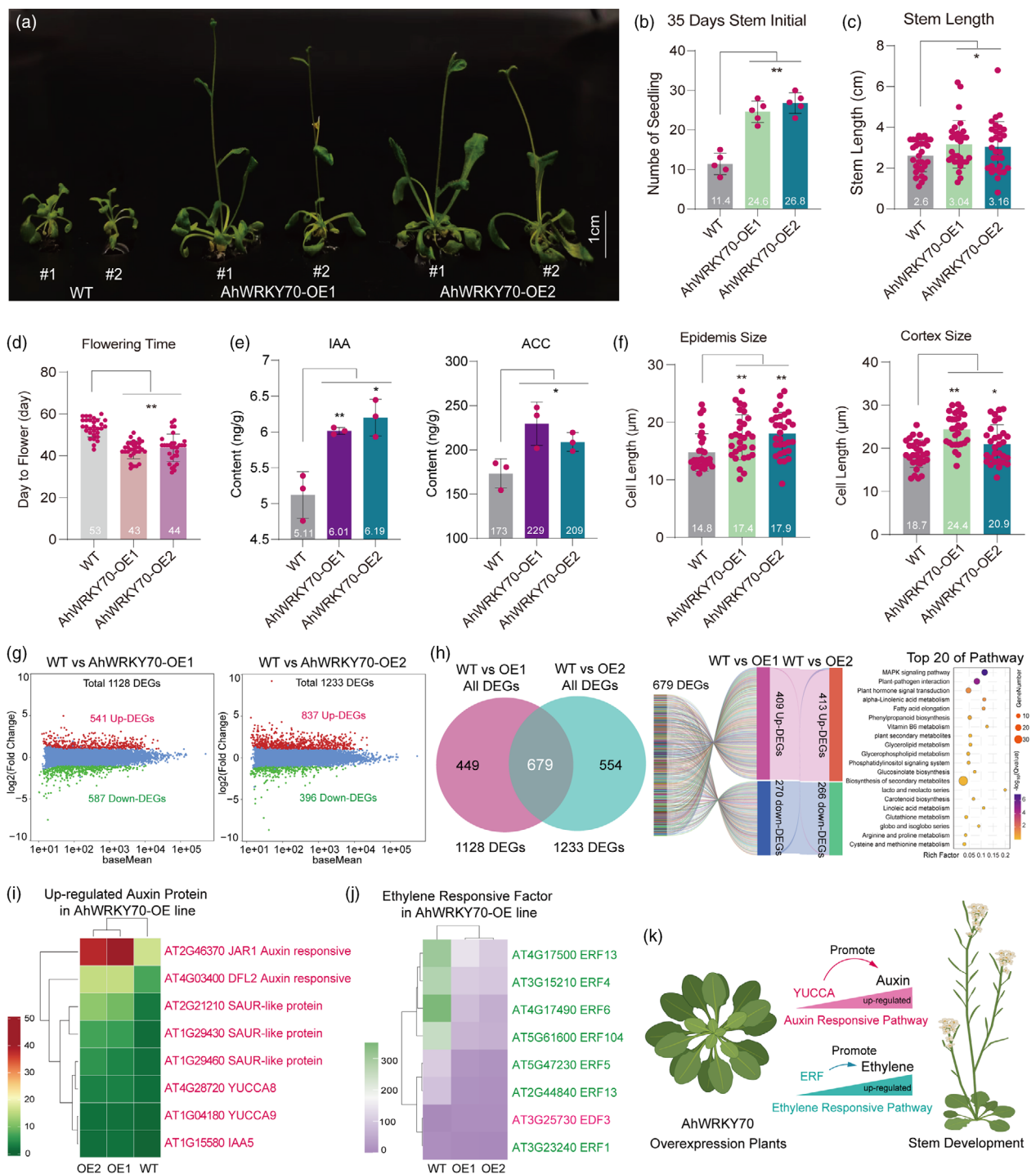


**Figure 8** Overexpression of *AhWRKY70* in *Arabidopsis* to validate the molecular function of *AhWRKY70* regulated plant stem development: (a) wild-type and *AhWRKY70-OE* plants growth phenotype, the *AhWRKY70-OE* line stem developed faster than wild-type at 35 days; (b) Investigation of the initial stem in wild-type and *AhWRKY70-OE* lines at 35 days (five biological repeats); (c) Investigation of stem length in wild-type and *AhWRKY70-OE* lines at 35 days ( $n = 30$ ); (d) Statistics of the day to flowering in wild-type and *AhWRKY70-OE* lines ( $n = 30$ ); (e) IAA and ACC content detection with three biological repeats in wild-type and *AhWRKY70-OE* lines with three biological repeats; (f) Epidermis and cortex cell size (cell diameter) in wild-type and *AhWRKY70-OE* lines ( $n = 30$ ) at 35 days; (g) RNA sequencing identified the distribution of differentially expressed genes in wild-type compared to two *AhWRKY70-OE* lines; (h) Expression dynamics and KEGG enrichment analysis (top 20 terms) of 679 co-DEGs in wild-type compared with *AhWRKY70-OE* lines; (i) Eight auxin responsive proteins expression levels in wild-type and *AhWRKY70-OE* lines; (j) Eight ethylene responsive factor expression levels in wild-type and *AhWRKY70-OE* lines; (k) An illustration that how the overexpression of *AhWRKY70* in *Arabidopsis* activates the auxin and ethylene pathways to promote the stem development in overexpressed plants as compared to normal plants. All statistical significance was indicated as  $*P < 0.05$  and  $**P < 0.01$  (*t*-test).

*et al.*, 2006) and *D14* (Yao *et al.*, 2018) re-associated with semi-dwarfism in rice, while *Rht* (Zhang *et al.*, 2023) determines stem length in wheat. *GID1* (Griffiths *et al.*, 2006) and *GAI* (Willige *et al.*, 2007) are key regulators of dwarfism. Despite these insights, the correlation between various hormones and the peanut stem elongation process remains incompletely characterized.

In this study, the analysis of exogenous hormones revealed that auxin and ACC levels increased significantly in one-week-old stems compared to three-day-old stems, indicating a strong association between auxin and peanut stem development. Furthermore, growth index measurements and histological sections showed notable changes in the cell size of the cortex during peanut stem growth. The proliferation of cortex cells primarily contributes to both the horizontal expansion and vertical elongation of the stem.

#### The single-nucleus RNA-seq (snRNA-seq) reveals the transcriptome atlas in different peanut tissues under single-cell resolution

In recent years, scRNA-seq has emerged as a powerful technology to reveal the heterogeneity of RNA transcripts within individual cells. Rare and novel cell types can be identified more quickly using scRNA-seq, allowing for the characterization of many different cell types and states and their roles in life processes to be more accurately and comprehensively understood (Shaw *et al.*, 2021). A number of articles have been published on the use of scRNA-seq technology to study *Arabidopsis* (Lopez-Anido *et al.*, 2021; Zhu *et al.*, 2023); and the single-cell transcriptome of peanut leaves has been reported, most of the major cell types in peanut leaf have been identified at single-cell resolution, and a novel hypothesis about cell differentiation in peanut leaf blade has been proposed (Liu *et al.*, 2021a). However, since plants have cell walls, protoplasts from plants are difficult to obtain. Therefore, the application of scRNA-seq technology in plant research is limited (Bawa *et al.*, 2022; Wang *et al.*, 2023). To address this issue, transcriptional profiles of single nuclear mRNA were obtained using the snRNA-seq method (Long *et al.*, 2021). snRNA-seq has now been applied to plants. For example, transcriptional profiles of different cell types in maize were obtained using snRNA-seq, describing signalling networks that control the movement and development of grass stomata (Sun *et al.*, 2022); high-resolution transcriptomic profiles describing nitrogen fixation and nodule development in soybean have been published (Sun *et al.*, 2023); it has been reported that the peanut leaf snRNA transcriptome atlas has been elucidated and the transcriptional regulatory network of leaf has been identified (Liu *et al.*, 2024). Although the snRNA-seq method has elucidated the development of many plant tissues (Farmer *et al.*, 2021; Li *et al.*, 2023a; Marand *et al.*, 2021), the development of the stem of peanut has not yet been elucidated. In this study, we expand the application scenarios of single-nuclei extraction and isolation in peanut stem, and this technique avoids the disadvantage of cell wall degradation with enzyme cellulase solution to expedite snRNA-seq application in another peanut tissues.

#### Peanut *AhWRKY70* regulates the plant stem development by integrating various phytohormone pathways

*WRKY* TFs are encoded by a multigene family and play vital roles in multiple biological processes during plant development. Usually, *WRKY* proteins contain the conserved WRKYGQK

sequence and zinc-finger motif, which specifically bind to the DNA motif of W-box elements (TTGACC/T). In *Arabidopsis thaliana*, *WRKY70* displays important but no indispensable roles in jasmonate and salicylic acid signalling. Modulation of *WRKY70* transcript levels by constitutive overexpression increases resistance to virulent pathogens and results in constitutive expression of SA-induced pathogenesis-related genes. Conversely, antisense suppression of *WRKY70* activates JA-responsive/COI1-dependent genes. Additionally, nonphosphorylated *WRKY70* binds a GACTTT motif in the *SARD1* promoter to prevent axenic activation of plant immunity by direct repression of *SARD1*. The binding of *WRKY70* to alternative cis-elements of *SARD1* through a phosphorylation-mediated switch controlled by *CHYR1* contributes to modulating the balance between immunity and growth (Liu *et al.*, 2021b; Ren *et al.*, 2008; Zhou *et al.*, 2018). Previous reports in model plants have shown that the *WRKY70* is a critically important factor for plants to control the trade-off between growth and pathogen immunity, but the underlying molecular mechanism of *WRKY70* remains largely unknown in leguminous crops.

Herein, we illustrated that the peanut *AhWRKY70* was localized to the nucleus and highly enriched in the stem cortex and xylem cell types, which expression level in distinct time-point presented negative correlation during the stem grown from 3 to 7 days. Although the phylogeny analysis displayed that the *AhWRKY70* was a homology of *Arabidopsis WRKY22* that promotes susceptibility to aphids and modulates salicylic acid and jasmonic acid signalling (Kloth *et al.*, 2016) the function background deficient of *WRKY22* in the regulation of plant growth was failed to provide a reference for understanding the *AhWRKY70* function. In this study, *AhWRKY70* showed a tissue-specific expression pattern, implying that *AhWRKY70* likely modulates multiple tissue development and also acts a regulator in stem growth. Further ectopic overexpression of *AhWRKY70* in *Arabidopsis* obviously promoted the stem development, and bolting earlier from the rosette tissue compared with wild-type plant, our investigation extended the understanding of *AhWRKY70* in the regulation of plant growth. However, whether *AhWRKY70* also regulates pathogen resistance in peanuts still needs to be validated in future studies.

## Materials and methods

### Peanut stem nucleus isolation

Peanut variety "Yueyou1823" collected from the Crops Research Institute of Guangdong Academy of Agriculture Science (GDAAS) was used as the experimental plant material. One-week-old peanut seedlings were grown in an incubator (25 °C, 12 h light-dark alternation). The stem samples were collected and mixed at 7 days (9:00 a.m.) after the seedling cotyledon is grown out from the soil. Approximately 1 g of fresh stem was ground into powder by freezing in liquid nitrogen. The extracted powder was transferred into 10 mL of nucleus isolation buffer (5% dextran T40, 0.4 M sucrose, 10 mM MgCl<sub>2</sub>, 1 mM DTT, 100 mM Tris-HCl pH 7.4, 2 U/μL RNase inhibitor and 0.1% Triton X-100) and centrifuged at 300 **g** for 1 min. The supernatants were filtered through miracloth (70 μm) and re-filtered through a 40-μm cell strainer (BD Falcon). After centrifugation at 2000 **g** for 5 min, the pellet was re-suspended in wash buffer (10 mL solution: 10 mM PBS, 1% BSA and 2 U/μL RNase inhibitor). The nucleus solution was stained by DAPI (10 μM) and loaded on a

flow cytometer (BD FACSAriaII) with a 70  $\mu\text{m}$  nozzle (20 psi). The gate selection of nucleus DAPI sorting was a small particle gate with FCS-A vs SSC-A mode to remove macroaggregated impurities (Conde et al., 2021; Sunaga-Franze et al., 2021; Xu et al., 2021), and the collected nucleus extraction concentration was adjusted to 1000 cells/ $\mu\text{l}$ .

### Library construction and sequencing

The snRNA-seq libraries were constructed using chromium single-cell 3' GEM (Gel Beads in-Emulsion) Library & Gel Bead Kit v3 by using the nucleus suspensions in accordance with the manufacturer's instructions. The snRNA-seq libraries were sequenced using the paired-end mode of an Illumina sequencing platform HiSeq2500. Two independent biological replicates designated as Stems 1 and 2 were used in the peanut stem single-nuclei RNA-seq experiment.

### Bioinformatics analysis

The snRNA-seq raw data was processed using the 10x Genomics software Cell Ranger version 2.0 to convert the raw files to FASTQ files and perform alignment, filtering, cell calling and quantification. The peanut reference genome (GCF\_003086295, available at [Peanutbase.org](https://peanutbase.org)) was used to perform splice-aware read alignments using Cell Ranger. The *t*-distributed t-SNE was generated by performing batch correction using Harmony (Korsunsky et al., 2019). Log-normalized matrices were loaded onto SingleR packages to annotate cell types using known cell markers. The Wilcoxon rank-sum test was used to identify stem cell-type markers (Liu et al., 2022) for each cluster in snRNA-seq and to determine the differential accessibility of each cluster (Butler et al., 2018). Seurat was used to integrate the snRNA-seq data to determine gene expression. Single-cell trajectories were constructed using Monocle Version 2 (Trapnell et al., 2014). The cell pseudo-time trajectories were calculated by using PAGA. For the identification of upregulated DEGs, gene expression fold changes of DEGs in divergent cell clusters were calculated using Log<sub>2</sub>FC (fold change). The threshold for upregulated DEGs was set as abs Log<sub>2</sub>FC >0.25, *P*-value <0.05. DEGs were selected for GO and KEGG enrichment analysis using the hypergeometric test on the Omicshare platform (Mu et al., 2024). The list of all expressed genes, including KEGG and GO IDs (Table S3), was used as the background file, while the DEGs or TFs served as the query list. Results were obtained with a significance threshold of *P*-value <0.05. The DEG sequences were queried against the *Arabidopsis* reference genome and downloaded from the TAIR database ([www.arabidopsis.org](http://www.arabidopsis.org)) to identify their most similar homologues in *Arabidopsis*, with matches filtered at *P*-value <0.05. Protein-protein interactions among TFs were analysed using STRING (Szklarczyk et al., 2021) and visualized with Cytoscape (Shannon et al., 2003).

### Phytohormone uptake and detection assay

Stem samples were collected at 3 DAG and 7 DAG (9:00 am local time) and ground using liquid nitrogen. The powder (50 mg) of each sample was mixed with isotopic internal standards and extracted with 1 mL of an extraction solvent mixture (-methanol/ultrapure water/formic acid = 15:4:1, v/v/v). The extraction solutions were concentrated and re-solubilized with 100  $\mu\text{L}$  of 80% methanol, filtered through a 0.22  $\mu\text{m}$  syringe membrane and placed in the injection vial. Qualitative and quantitative phytohormone profiles were determined using ultra-

performance liquid chromatography–tandem mass spectrometry (UPLC-MS/MS) with internal isotopic standards. The details of isotopic internal standards used in the phytohormone experiment are listed in Table S15, sheet 2. Each assay was performed with triplicate independent repeats.

### Tissue bulk RNA-seq

Peanut seedling stems were harvested at 3 and 7 days. Stems from at least five independent plants exhibiting the same growth phenotype were pooled for total RNA extraction using TRIzol reagent (Invitrogen). Total RNA was used for library construction following the high-throughput illumina strand-specific RNA sequencing library protocol. The RNA libraries were sequenced on an Illumina HiSeq2000 to produce 200-bp paired-end reads; each sample had three biological repeats. The last assembled reads were mapped to the peanut genome database (GCF\_003086295, available at [Peanutbase.org](https://peanutbase.org)) by using Tophat. Cufflinks software (version 2.2.1) was used to compute the relative expression of total genes. The FPKM (fragments per kilobase of transcript per million fragments mapped) values were extracted using featureCounts (version 2.0.1) to measure gene expression levels (Liao et al., 2014). The expression matrix was imported into R (version 4.1.0) for differential gene expression analysis using the DESeq2 package (version 1.32.0), a method based on the negative binomial distribution (Love et al., 2014). Genes with an adjusted *P*-value <0.05 and a Log<sub>2</sub> fold change (FC)  $\geq |1|$  were considered and differentially expressed. These genes were further analysed for GO and KEGG enrichment using a hypergeometric test-based tool on the Omicshare platform (Mu et al., 2024). Using KEGG and GO IDs as the background, DEGs were submitted for enrichment analysis with a significance threshold of *P*-value <0.05 (Table S11). In the bulk RNA-seq analysis of peanut stem tissue, day 3 stem tissue served as the control group. DEGs were identified by comparing gene expression profiles on day 7 with those on day 3 in whole peanut seedling stem tissue.

### Total RNA extraction, quantitative real-time PCR analysis of gene expression

Total RNA was extracted from 100 mg of peanut stem using Trizol Reagent (Invitrogen, Carlsbad, CA, USA) and then reverse-transcribed using a PrimeScript RT reagent Kit (TOYOBO FSK-100, Shanghai, China) following the protocol. The cDNA was quantified in a 20- $\mu\text{L}$  reaction volume with SYBR Premix ExTaq™ (TaKaRa, Beijing, China) by using the ABI StepOne Plus system. The relative gene expression levels as FC compared to control sample were calculated using the 2<sup>-ΔΔCT</sup> calculating method. Samples were collected as three biological replicates (Deng et al., 2024).

### Phylogenetic analysis, subcellular localization and overexpression of *AhWRKY70* gene in *Arabidopsis thaliana*

The homologous *AhWRKY70* gene was searched by NCBI protein BLAST, and a phylogenetic tree was constructed using MEGA version 7 (Tamura et al., 2013). The CDS sequence of *AhWRKY70* without the stop codon was inserted into the plasmid vector containing green fluorescent protein pBWA(V)HS-GFP. The fusion expression vector pBWA(V)HS-*AhWRKY70*-GFP with the *AhWRKY70* gene was constructed. pBWA(V)HS-*AhWRKY70*-GFP vector was transformed into *Arabidopsis* protoplasts using polyethylene glycol at 28 °C for 18 h in dark culture, and slides

were prepared and placed under a laser confocal microscope (Nikon C2-ER, Japan) for observation.

Subsequently, in order to generate transgenic plants, the CDS sequence of *AhWRKY70* was cloned into the pBWA(V)HS plasmid vector to construct the 35S-*AhWRKY70* plasmid, which was transformed into *Agrobacterium tumefaciens* strain EHA105 to infiltrate inflorescence using the *Agrobacterium*-mediated floral dipping method in *Arabidopsis*. The true transformed T0 seeds were selected by hygromycin (Hyg), and stable *AhWRKY70* overexpressed lines were obtained at T2 generation (Liu et al., 2021a). We used the *AhWRKY70*-OE (*AhWRKY70* over-expressed) lines to record stem initial growth phenotypes. *Arabidopsis* (ecotype Columbia) species were used as wild type to compare the phenotypes of transgenic *Arabidopsis* lines with wild type.

## Acknowledgements

This work was supported by The National Key R&D Program of China (2023YFD1202800), the Open Competition Program of Top Ten Critical Priorities of Agricultural Science and Technology Innovation for the 14th Five-Year Plan in Guangdong Province (2022SDZG05), Guangdong Provincial Key Research and Development Program-Modern Seed Industry (2022B0202060004), China Agriculture Research System of MOF and MARA (CARS-13), the National Natural Science Foundation of China (32 172 051 and 32 301 869), Guangdong Science and Technology Plan Project (2023B1212060038), Guangdong Basic and Applied Basic Research Foundation (2023A1515010098), Technology Special Fund of Guangdong Province Agriculture and Rural Affairs Department (2019KJ136-02), Special Funds for the Revitalization of Agriculture through Seed Industry under the Provincial Rural Revitalization Strategy (2022-NPY-00-022), Guangzhou Basic and Applied Basic Research Foundation (202 201 010 281 and 2023A04J0776), Special Fund for Scientific Innovation Strategy-Construction of High Level Academy of Agriculture Science (R2020PY-JX004, R2020PY-JG005, R2021PY-QY003, R2022YJ-YB3025 and R2023PY-JG007), the Project of Collaborative Innovation Center of GDAAS (XTXM202203), Science and Technology Planning Project of Heyuan City (Heyuan She Nong DaZhuan Xiang 2 022 002) and Science and Technology Project of Qingyuan City 2023 (2023KJJ002).

## Conflict of interests

The authors declare no competing interests.

## Author contributions

Xinyang Wang, Xing Huo, Hao Liu written the manuscript draft; Muhammad J. Umer improve the manuscript quality with language editing; Runfeng Wang and Yueni Zhou validated the molecular function of *AhWRKY70*; Zihao Zheng provided the bioinformatics analysis for the single-nuclei RNA-seq; Lu Huang provided the data analysis of bulk RNA-seq; Haifen Li, Qianxia Yu and Shaoxiong Li isolated the single-nuclei in peanut stem and obtained the snRNA-seq raw data; Wenyi Wang and Weicai Jin provided the supporting for the qPCR, hormone examination, histologic section; Rajeev Varshney conceived and interpreted the experiments; Yuan Xiao helped to revise the improved manuscript version; Hao Liu, Qing Lu, Xiaoping Chen and Yanbin Hong obtained the foundation.

## Data availability statement

The raw sequence data reported in this work have been deposited in the Genome Sequence Archive (GSA) in National Genomics Data Center (NGDC), China National Center for Bioinformation Beijing Institute of Genomics and Chinese Academy of Sciences. Peanut seedling stem tissue bulk RNA-seq raw data (GSA: CRA014839) and peanut stem snRNA-seq raw data (GSA: CRA014837) are publicly accessible on the NGDC database.

## References

- Asano, K., Yamasaki, M., Takuno, S., Miura, K., Katagiri, S., Ito, T., Doi, K. et al. (2011) Artificial selection for a green revolution gene during japonica rice domestication. *Proc. Natl. Acad. Sci. USA* **108**, 11034–11039.
- Balkunde, R., Kitagawa, M., Xu, X.M., Wang, J. and Jackson, D. (2017) SHOOT MERISTEMLESS trafficking controls axillary meristem formation, meristem size and organ boundaries in *Arabidopsis*. *Plant J.* **90**, 435–446.
- Bawa, G., Liu, Z., Yu, X., Qin, A. and Sun, X. (2022) Single-cell RNA sequencing for plant research: insights and possible benefits. *Int. J. Mol. Sci.* **23**, 4497.
- Butler, A., Hoffman, P., Smibert, P., Papalexi, E. and Satija, R. (2018) Integrating single-cell transcriptomic data across different conditions, technologies, and species. *Nat. Biotechnol.* **36**, 411–420.
- Chen, X., Lu, Q., Liu, H., Zhang, J., Hong, Y., Lan, H., Li, H. et al. (2019) Sequencing of cultivated peanut, *Arachis hypogaea*, yields insights into genome evolution and oil improvement. *Mol. Plant* **12**, 920–934.
- Chow, C.N., Yang, C.W., Wu, N.Y., Wang, H.T., Tseng, K.C., Chiu, Y.H., Lee, T.Y. et al. (2024) PlantPAN 4.0: updated database for identifying conserved non-coding sequences and exploring dynamic transcriptional regulation in plant promoters. *Nucleic Acids Res.* **52**(D1), D1569–D1578.
- Conde, D., Triziozzi, P.M., Balmant, K.M., Doty, A.L., Miranda, M., Boullosa, A., Schmidt, H.W. et al. (2021) A robust method of nuclei isolation for single-cell RNA sequencing of solid tissues from the plant genus *Populus*. *PLoS One* **16**, e251149.
- Deng, Q., Du, P., Gangurde, S.S., Hong, Y., Xiao, Y., Hu, D., Li, H. et al. (2024) ScRNA-seq reveals dark- and light-induced differentially expressed gene atlases of seedling leaves in *Arachis hypogaea* L. *Plant Biotechnol. J.* **22**, 1848–1866.
- Du, P., Deng, Q., Wang, W., Garg, V., Lu, Q., Huang, L., Wang, R. et al. (2023) scRNA-seq reveals the mechanism of fatty acid desaturase 2 mutation to repress leaf growth in peanut (*Arachis hypogaea* L.). *Cells* **12**(18), 2305.
- Farmer, A., Thibivilliers, S., Ryu, K.H., Schiefelbein, J. and Libault, M. (2021) Single-nucleus RNA and ATAC sequencing reveals the impact of chromatin accessibility on gene expression in *Arabidopsis* roots at the single-cell level. *Mol. Plant* **14**, 372–383.
- Furze, M.E., Trumbore, S. and Hartmann, H. (2018) Detours on the phloem sugar highway: stem carbon storage and remobilization. *Curr. Opin. Plant Biol.* **43**, 89–95.
- Greb, T. and Lohmann, J.U. (2016) Plant stem cells. *Curr. Biol.* **26**, R816–R821.
- Griffiths, J., Murase, K., Rieu, I., Zentella, R., Zhang, Z.L., Powers, S.J., Gong, F. et al. (2006) Genetic characterization and functional analysis of the GID1 gibberellin receptors in *Arabidopsis*. *Plant Cell* **18**, 3399–3414.
- Hirakawa, Y. (2021) CLAVATA3, a plant peptide controlling stem cell fate in the meristem. *Peptides* **142**, 170579.
- Hunziker, P. and Greb, T. (2024) Stem cells and differentiation in vascular tissues. *Annu. Rev. Plant Biol.* **75**, 399–425.
- Jha, P., Ochatt, S.J. and Kumar, V. (2020) WUSCHEL: a master regulator in plant growth signaling. *Plant Cell Rep.* **39**, 431–444.
- Kloth, K.J., Wiegers, G.L., Busscher-Lange, J., van Haarst, J.C., Kruijer, W., Bouwmeester, H.J., Dicke, M. et al. (2016) AtWRKY22 promotes susceptibility to aphids and modulates salicylic acid and jasmonic acid signalling. *J. Exp. Bot.* **67**, 3383–3396.
- Korangi, A.V., Argüelles, A.A., Ribeiro, B., De Coninck, B., Helmus, C., Delaplace, P. and Ongena, M. (2023) *Bacillus* lipopeptide-mediated biocontrol of peanut stem rot caused by *Athelia rolfsii*. *Front. Plant Sci.* **14**, 1069971.

- Korsunsky, I., Millard, N., Fan, J., Slowikowski, K., Zhang, F., Wei, K., Baglaenko, Y. et al. (2019) Fast, sensitive and accurate integration of single-cell data with Harmony. *Nat. Methods* **16**, 1289–1296.
- Kuroha, T., Nagai, K., Gamuyao, R., Wang, D.R., Furuta, T., Nakamori, M., Kitaoka, T. et al. (2018) Ethylene-gibberellin signaling underlies adaptation of rice to periodic flooding. *Science* **361**, 181–186.
- Li, C., Zhang, S., Yan, X., Cheng, P. and Yu, H. (2023a) Single-nucleus sequencing deciphers developmental trajectories in rice pistils. *Dev. Cell* **58**, 694–708.
- Li, L., Wang, J., Liu, D., Li, L., Zhen, J., Lei, G., Wang, B. et al. (2023b) The antagonistic potential of peanut endophytic bacteria against *Sclerotium rolfsii* causing stem rot. *Braz. J. Microbiol.* **54**, 361–370.
- Liao, R.Y. and Wang, J.W. (2023) Analysis of meristems and plant regeneration at single-cell resolution. *Curr. Opin. Plant Biol.* **74**, 102378.
- Liao, Y., Smyth, G.K. and Shi, W. (2014) featureCounts: an efficient general purpose program for assigning sequence reads to genomic features. *Bioinformatics* **30**, 923–930.
- Liu, H., Guo, Z., Gangurde, S.S., Garg, V., Deng, Q., Du, P., Lu, Q. et al. (2024) A single-nucleus resolution atlas of transcriptome and chromatin accessibility for peanut (*Arachis hypogaea* L.) leaves. *Advanced Biology* **8**, e2300410.
- Liu, H., Hu, D., Du, P., Wang, L., Liang, X., Li, H., Lu, Q. et al. (2021a) Single-cell RNA-seq describes the transcriptome landscape and identifies critical transcription factors in the leaf blade of the allotetraploid peanut (*Arachis hypogaea* L.). *Plant Biotechnol. J.* **19**, 2261–2276.
- Liu, H., Liu, B., Lou, S., Bi, H., Tang, H., Tong, S., Song, Y. et al. (2021b) CHYR1 ubiquitinates the phosphorylated WRKY70 for degradation to balance immunity in *Arabidopsis thaliana*. *New Phytol.* **230**, 1095–1109.
- Liu, Y., Li, C., Han, Y., Li, R., Cui, F., Zhang, H., Su, X. et al. (2022) Spatial transcriptome analysis on peanut tissues shed light on cell heterogeneity of the peg. *Plant Biotechnol. J.* **20**, 1648–1650.
- Long, Y., Liu, Z., Jia, J., Mo, W., Fang, L., Lu, D., Liu, B. et al. (2021) FlsnRNA-seq: protoplasting-free full-length single-nucleus RNA profiling in plants. *Genome Biol.* **22**, 66.
- Lopez-Anido, C.B., Vatén, A., Smoot, N.K., Sharma, N., Guo, V., Gong, Y., Anleu, G.M. et al. (2021) Single-cell resolution of lineage trajectories in the *Arabidopsis* stomatal lineage and developing leaf. *Dev. Cell* **56**, 1043–1055.
- Love, M.I., Huber, W. and Anders, S. (2014) Moderated estimation of fold change and dispersion for RNA-seq data with DESeq2. *Genome Biol.* **15**, 550.
- Lu, Q., Huang, L., Liu, H., Garg, V., Gangurde, S.S., Li, H., Chitikineni, A. et al. (2024) A genomic variation map provides insights into peanut diversity in China and associations with 28 agronomic traits. *Nat. Genet.* **56**, 530–540.
- Marand, A.P., Chen, Z., Gallavotti, A. and Schmitz, R.J. (2021) A cis-regulatory atlas in maize at single-cell resolution. *Cell* **184**, 3041–3055.
- Mu, H., Chen, J., Huang, W., Huang, G., Deng, M., Hong, S., Ai, P. et al. (2024) OmicShare tools: a zero-code interactive online platform for biological data analysis and visualization. *Imeta* **3**, e228.
- Peng, L., Liu, H., Wu, Y., Bing, J. and Zhang, G. (2024) New advances in the regulation of stem growth in vascular plants. *Plant Growth Regul.* **103**(1), 65–80.
- Ren, C.M., Zhu, Q., Gao, B.D., Ke, S.Y., Yu, W.C., Xie, D.X. and Peng, W. (2008) Transcription factor WRKY70 displays important but no indispensable roles in jasmonate and salicylic acid signaling. *J. Integr. Plant Biol.* **50**, 630–637.
- Rodriguez-Villalon, A. and Brady, S.M. (2019) Single cell RNA sequencing and its promise in reconstructing plant vascular cell lineages. *Curr. Opin. Plant Biol.* **48**, 47–56.
- Ryu, K.H., Zhu, Y. and Schiefelbein, J. (2021) Plant cell identity in the era of single-cell transcriptomics. *Annu. Rev. Genet.* **55**, 479–496.
- Sakamoto, T., Morinaka, Y., Ohnishi, T., Sunohara, H., Fujioka, S., Ueguchi-Tanaka, M., Mizutani, M. et al. (2006) Erect leaves caused by brassinosteroid deficiency increase biomass production and grain yield in rice. *Nat. Biotechnol.* **24**, 105–109.
- Serrano-Mislata, A. and Sablowski, R. (2018) The pillars of land plants: new insights into stem development. *Curr. Opin. Plant Biol.* **45**, 11–17.
- Shannon, P., Markiel, A., Ozier, O., Baliga, N.S., Wang, J.T., Ramage, D., Amin, N. et al. (2003) Cytoscape: a software environment for integrated models of biomolecular interaction networks. *Genome Res.* **13**, 2498–2504.
- Shaw, R., Tian, X. and Xu, J. (2021) Single-cell transcriptome analysis in plants: advances and Challenges. *Mol. Plant* **14**, 115–126.
- Sinha, P., Bajaj, P., Pazhamala, L.T., Nayak, S.N., Pandey, M.K., Chitikineni, A., Huai, D. et al. (2020) *Arachis hypogaea* gene expression atlas for fastigia subspecies of cultivated groundnut to accelerate functional and translational genomics applications. *Plant Biotechnol. J.* **18**, 2187–2200.
- Sun, B., Wang, Y., Yang, Q., Gao, H., Niu, H., Li, Y., Ma, Q. et al. (2023) A high-resolution transcriptomic atlas depicting nitrogen fixation and nodule development in soybean. *J. Integr. Plant Biol.* **65**, 1536–1552.
- Sun, G., Xia, M., Li, J., Ma, W., Li, Q., Xie, J., Bai, S. et al. (2022) The maize single-nucleus transcriptome comprehensively describes signaling networks governing movement and development of grass stomata. *Plant Cell* **34**, 1890–1911.
- Sunaga-Franze, D.Y., Muino, J.M., Braeuning, C., Xu, X., Zong, M., Smacznia, C., Yan, W. et al. (2021) Single-nucleus RNA sequencing of plant tissues using a nanowell-based system. *Plant J.* **108**, 859–869.
- Szklarczyk, D., Gable, A.L., Nastou, K.C., Lyon, D., Kirsch, R., Pyysalo, S., Doncheva, N.T. et al. (2021) The STRING database in 2021: customizable protein-protein networks, and functional characterization of user-uploaded gene/measurement sets. *Nucleic Acids Res.* **49**, D605–D612.
- Tamura, K., Stecher, G., Peterson, D., Filipski, A. and Kumar, S. (2013) MEGA6: molecular evolutionary genetics analysis version 6.0. *Mol. Biol. Evol.* **30**, 2725–2729.
- Trapnell, C., Cacchiarelli, D., Grimsby, J., Pokharel, P., Li, S., Morse, M., Lennon, N.J. et al. (2014) The dynamics and regulators of cell fate decisions are revealed by pseudotemporal ordering of single cells. *Nat. Biotechnol.* **32**, 381–386.
- Wang, K., Zhao, C., Xiang, S., Duan, K., Chen, X., Guo, X. and Sahu, S.K. (2023) An optimized FACS-free single-nucleus RNA sequencing (snRNA-seq) method for plant science research. *Plant Sci.* **326**, 111535.
- Willige, B.C., Ghosh, S., Nill, C., Zourelidou, M., Dohmann, E.M., Maier, A. and Schwechheimer, C. (2007) The DELLA domain of GA INSENSITIVE mediates the interaction with the GA INSENSITIVE DWARF1A gibberellin receptor of *Arabidopsis*. *Plant Cell* **19**, 1209–1220.
- Xu, W., Wen, Y., Liang, Y., Xu, Q., Wang, X., Jin, W. and Chen, X. (2021) A plate-based single-cell ATAC-seq workflow for fast and robust profiling of chromatin accessibility. *Nat. Protoc.* **16**, 4084–4107.
- Yan, L., Song, W., Wang, Z., Yu, D., Sudini, H., Kang, Y., Lei, Y. et al. (2023) Dissection of the genetic basis of resistance to stem rot in cultivated peanuts (*Arachis hypogaea* L.) through genome-wide association study. *Genes* **14**(7), 1447.
- Yao, R., Wang, L., Li, Y., Chen, L., Li, S., Du, X., Wang, B. et al. (2018) Rice DWARF14 acts as an unconventional hormone receptor for strigolactone. *J. Exp. Bot.* **69**, 2355–2365.
- Ye, J., Tian, R., Meng, X., Tao, P., Li, C., Liu, G., Chen, W. et al. (2020) Tomato SD1, encoding a kinase-interacting protein, is a major locus controlling stem development. *J. Exp. Bot.* **71**, 3575–3587.
- Yu, K., Oliver, J., McKinley, B., Weers, B., Fabich, H.T., Evertt, N., Conradi, M.S. et al. (2022) Bioenergy sorghum stem growth regulation: intercalary meristem localization, development, and gene regulatory network analysis. *Plant J.* **112**, 476–492.
- Zang, X., Liu, J., Zhao, J., Liu, J., Ren, J., Li, L., Li, X. et al. (2023) Uncovering mechanisms governing stem growth in peanut (*Arachis hypogaea* L.) with varying plant heights through integrated transcriptome and metabolomics analyses. *J. Plant Physiol.* **287**, 154052.
- Zhang, J., Li, C., Zhang, W., Zhang, X., Mo, Y., Tranquilli, G.E., Vanzetti, L.S. et al. (2023) Wheat plant height locus RHT25 encodes a PLATZ transcription factor that interacts with DELLA (RHT1). *Proc. Natl. Acad. Sci. USA* **120**, e1994764176.
- Zhou, M., Lu, Y., Bethke, G., Harrison, B.T., Hatsugai, N., Katagiri, F. and Glazebrook, J. (2018) WRKY70 prevents axenic activation of plant immunity by direct repression of SARD1. *New Phytol.* **217**, 700–712.
- Zhou, X., Jiang, Y. and Yu, D. (2011) WRKY22 transcription factor mediates dark-induced leaf senescence in *Arabidopsis*. *Mol. Cells* **31**, 303–313.

Zhu, J., Lolle, S., Tang, A., Guel, B., Kvitko, B., Cole, B. and Coaker, G. (2023) Single-cell profiling of *Arabidopsis* leaves to *Pseudomonas syringae* infection. *Cell Rep.* **42**, 112676.

## Supporting information

Additional supporting information may be found online in the Supporting Information section at the end of the article.

**Figure S1** Average gene number and UMI in all peanut cells by snRNA-seq identification.

**Figure S2** Cell clusters and cell numbers in peanut stem identified by snRNA-seq.

**Figure S3** Identification of specific up-regulated DEGs in each cell cluster.

**Figure S4** KEGG enrichment analysis of identified cell types in peanut stem.

**Figure S5** GO analysis in identified cell types of peanut stem.

**Figure S6** Expression levels of 14 newly identified marker genes in stem bulk RNA-seq profiles comparing 7-day and 3-day samples.

**Figure S7** Expression level and trend analysis of 85 core transcription factors (TFs) in stem cell types.

**Figure S8** Cell differentiation state of all identified cell-type cells.

**Figure S9** Cell differentiation state analysis in distinct cell types.

**Figure S10** Validation of 12 core transcription factors (TFs) in stem tissue at 3 and 7 days by quantitative real-time qPCR.

**Figure S11** Cell-cycle analysis of peanut stem cells.

**Figure S12** Relative expression level of *AhWRKY70* in different peanut tissues by quantitative real-time PCR.

**Figure S13** *AhWRKY70* promoter sequence with two different mutant sites at the position of -1272 bp.

**Figure S14** The relative expression of *AhWRKY70* in the *Arabidopsis* transgenic plants.

**Figure S15** Histologic section of stem in *AhWRKY70*-OE lines and wild-type plant.

**Figure S16** Statistics analysis of stem vascular cell size and pith cell size in *AhWRKY70*-OE lines and wild-type plant.

**Table S1** The data quality control of single-nuclei RNA sequencing (snRNA-seq) in peanut stem.

**Table S2** Statistics analysis of stem cell in snRNA-seq identified cell cluster.

**Table S3** snRNA-seq identified all expressed genes in each cell cluster of peanut stem.

**Table S4** snRNA-seq identified all DEGs in each peanut stem cell cluster.

**Table S5** snRNA-seq identified all DEGs in five cell types of peanut stem.

**Table S6** DEGs identification in peanut stem cell development trajectory.

**Table S7** DEGs identification in peanut stem cell differentiation state.

**Table S8** DEGs identification in peanut stem cell differentiation fate.

**Table S9** DEGs identification in peanut stem cell development trajectory by PAGA model.

**Table S10** DEGs identification in five peanut stem cell-type development trajectory.

**Table S11** Bulk RNA-seq identified all expressed genes in distinct time-point during stem development from 3 to 7 days.

**Table S12** DEGs identification in peanut stem at different growth time-points (7 days vs. 3 days) by bulk RNA-seq.

**Table S13** 763 DEGs identification in the profile of peanut stem cell-type DEGs compared with bulk RNA-seq DEGs.

**Table S14** DEGs identification in stem cell cycle.

**Table S15** Hormone content examination in peanut stem at different growth time-points (7 days vs. 3 days).

**Table S16** Conserved DNA-binding motif prediction at the position of -1272 bp in the *AhWRKY70* promoter region.

**Table S17** Hormone content examination in stem of *AhWRKY70*-OE and wild-type plants.

**Table S18** Bulk RNA-seq identified the DEGs in stem of *AhWRKY70*-OE and wild-type plants.

**Table S19** Six hundred seventy-nine co-DEGs in two *AhWRKY70*-OE and wild-type plants by bulk RNA-seq analysis.